ISSN 2413-9432

BIOMEDICAL PHOTONICS

Volume 11, # 2, 2022

In the issue:

- Cancer cell survival model after photodynamic therapy
- Application of biophantomes to evaluate the thermal effects of laser radiation with wavelengths of 970 nm and 1560 nm under different exposure modes
- Study of acute toxicity of monocationic chlorin e6 derivative, a perspective photosensitizer for antimicrobial and antitumor photodynamic therapy
- Opportunities of using oral intraluminal laser lithotripsy for a large calculus of the common bile duct (clinical report)

BMP

Российская Фотодинамическая Ассоциация

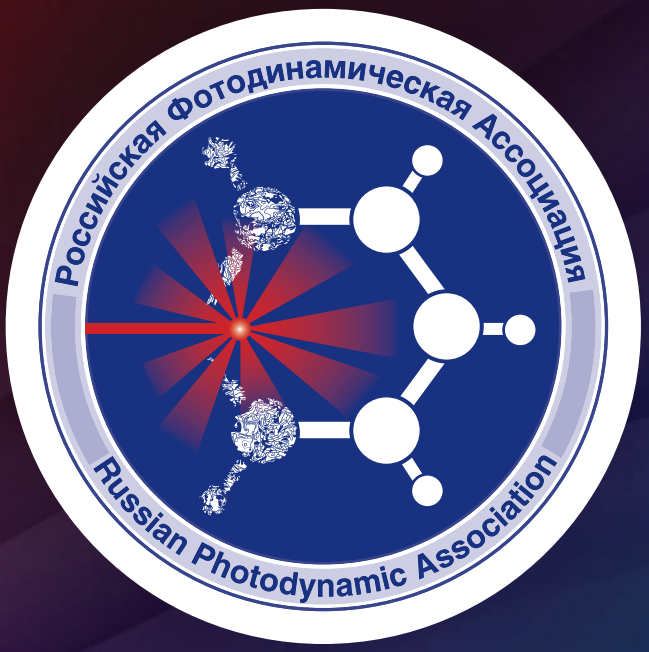

www.pdt-association.com

BIOMEDICAL PHOTONICS

BIOMEDICAL PHOTONICS –
research and practice, peer-reviewed, multidisciplinary journal.
The journal is issued 4 times per year.
The circulation – 1000 copies., on a quarterly basis.

The journal is included into the List of peer-reviewed science press of the State Commission for Academic Degrees and Titles of Russian Federation
The journal is indexed in the international abstract and citation database – Scopus.

The publisher «Agentstvo MORE».
Moscow, Khokhlovskiy lane., 9

Editorial staff:
Chief of the editorial staff Ivanova-Radkevich V.I.
Science editor professor Mamontov A.S.

Literary editor	Moiseeva R.N.
Translators	Urlova A.N.
	Romanishkin I.D.
Computer design	Kreneva E.I.
Desktop publishing	Merkulova O.E.

The Address of Editorial Office:
Russia, Moscow, 2nd Botkinskiy proezd, 3
Tel. 8 (495) 945–86–60
www: PDT-journal.com
E-mail: PDT-journal@mail.ru

Corresponding to:
125284, Moscow, p/o box 13

Registration certificate ПИ № ФС 77–51995, issued on 29.11.2012 by the Federal Service for Supervision of Communications, Information Technology, and Mass Media of Russia

The subscription index of «Rospechat» agency – 70249

BIOMEDICAL PHOTONICS

BIOMEDICAL PHOTONICS –
научно-практический, рецензируемый, мультидисциплинарный журнал.
Выходит 4 раза в год.
Тираж – 1000 экз., ежеквартально.

Входит в Перечень ведущих рецензируемых научных журналов ВАК РФ.
Индексируется в международной реферативной базе данных Scopus.

Издательство «Агентство МОРЕ».
Москва, Хохловский пер., д. 9

Редакция:

Зав. редакцией	Иванова-Радкевич В.И.
Научный редактор	проф. Мамонтов А.С.
Литературный редактор	Моисеева Р.Н.
Переводчики	Урлова А.Н.
	Романишкин И.Д.
Компьютерный дизайн	Кренева Е.И.
Компьютерная верстка	Меркулова О.Е.

Адрес редакции:
Россия, Москва, 2-й Боткинский пр., д. 3
Тел. 8 (495) 945–86–60
www: PDT-journal.com
E-mail: PDT-journal@mail.ru

Адрес для корреспонденции:
125284, Москва, а/я 13

Свидетельство о регистрации ПИ
№ ФС 77–51995, выдано 29.11.2012 г. Федеральной службой по надзору в сфере связи, информационных технологий
и массовых коммуникаций (Роскомнадзор)

Индекс по каталогу агентства «Роспечать» – 70249

ORIGINAL ARTICLES

Cancer cell survival model after photodynamic therapy
Karami-Gadallo L., Pouladian M. 4

Application of biophantomes to evaluate the thermal effects of laser radiation with wavelengths of 970 nm and 1560 nm under different exposure modes
Ostreiko O.V., Galkin M.A., Papayan G.V., Grishacheva T.G., Petrishchev N.N. 12

Study of acute toxicity of monocationic chlorin e6 derivative, a perspective photosensitizer for antimicrobial and antitumor photodynamic therapy
Zhidomorov N.Yu., Nazarenko O.A., Demidov V.I., Kustov A.V., Kukushkina N.V., Koifman O.I., Gagua A.K., Tomilova I.K., Berezin D.B. 23

CASE REPORTS

Opportunities of using oral intraluminal laser lithotripsy for a large calculus of the common bile duct (clinical report)
Ivanov Y.V., Sazonov D.V., Smirnov A.V., Mamoshin A.V., Baranov A.V., Panchenkov D.N. 33

ОРИГИНАЛЬНЫЕ СТАТЬИ

Модель выживаемости опухолевых клеток после фотодинамической терапии
L. Karami-Gadallo, M. Pouladian 4

Применение биофантомов для оценки термических эффектов лазерного излучения с длинами волн 970 нм и 1560 нм при разных режимах воздействия
О.В. Острейко, М.А. Галкин, Г.В. Папаян, Т.Г. Гришачева, Н.Н. Петрищев 12

Исследование острой токсичности монокатионного производного хлорина е6 – перспективного фотосенсибилизатора для антимикробной и противоопухолевой фотодинамической терапии
Н.Ю. Жидоморов, О.А. Назаренко, В.И. Демидов, А.В. Кустов, Н.В. Кукушкина, О.И. Койфман, А.К. Гагуа, И.К. Томилова, Д.Б. Березин 23

КЛИНИЧЕСКИЕ НАБЛЮДЕНИЯ

Возможности применения пероральной внутрипросветной лазерной литотрипсии при крупном конкременте общего желчного протока (клиническое наблюдение)
Ю.В. Иванов, Д.В. Сазонов, А.В. Смирнов, А.В. Мамошин, А.В. Баранов, Д.Н. Панченков 33

ORIGINAL ARTICLES

CANCER CELL SURVIVAL MODEL AFTER PHOTODYNAMIC THERAPY

Karami-Gadallo L., Pouladian M.
Islamic Azad University, Tehran, Iran

Abstract

Photodynamic therapy (PDT) is known as a routine treatment method in which cell survival index like viability plotted versus $^1O_2$ concentration or light fluence in the form of a curve. In this paper, a mathematical model was proposed with ability of generating a mirrored-sigmoid curve which seems to be fitted to any experimental data relating to cell viability, survival probability or any cellular index representing living conditions through adjusting three parameters. It was validated by showing an excellent curve fitting relatively with data obtained from cancerous lung cells under ALA-PDT process in vitro.

It was tried to define the relations between model's parameters and biological/clinical factors with the curve regions of plateau (at low doses; non-sensitive part), steep (high-sensitive part), and steady state (at high doses; low-sensitive part). It seems this model could be excellently fitted to any data presenting the cell-living index versus the killer agent in «any cancer therapy technique (e.g. radiotherapy)». Although this claim showed to be correct for PDT, different relevant data of other researchers should also be used for this model and other usual models too, in order to compare their fitness rates.

Key words: cell survival curve, mathematical modeling, photodynamic therapy.

For citations: Karami-Gadallo L., Pouladian M. Cancer cell survival model after photodynamic therapy, *Biomedical Photonics*, 2022, vol. 11, no. 2, pp. 4–11. doi: 10.24931/2413–9432–2022–11-2–4–11.

Contacts: L. Karami-Gadallo, e-mail: leilakarami271@yahoo.com

МОДЕЛЬ ВЫЖИВАЕМОСТИ ОПУХОЛЕВЫХ КЛЕТОК ПОСЛЕ ФОТОДИНАМИЧЕСКОЙ ТЕРАПИИ

L. Karami-Gadallo, M. Pouladian
Исламский Университет Азад, Тегеран, Иран

Резюме

При проведении фотодинамической терапии (ФДТ) индекс выживаемости (жизнеспособность) клеток в зависимости от концентрации $^1O_2$ или плотности мощности облучения на графике представляет собой кривую. В этой статье была предложена математическая модель с возможностью построения зеркально-сигмовидной кривой, которая, по мнению авторов, может быть использована для любых экспериментальных данных, касающихся жизнеспособности клеток или вероятности выживания, путем настройки трех параметров. Это было подтверждено демонстрацией совпадения кривой с данными, полученными в эксперименте *in vitro* для ФДТ с 5-аминолевулиновой кислотой клеток рака легкого.

Была предпринята попытка определить взаимосвязь между параметрами биологической модели и формой участков кривой. При низких дозах наблюдали на кривой участок плато (нечувствительная часть), при средних дозах – участок крутого подъема (высокочувствительная часть) и при высоких дозах – стационарное состояние (низкочувствительная часть). Авторы считают, что предложенная ими модель может быть применена к описанию любых данных, представляющих собой показатель выживаемости клеток, в зависимости от дозы воздействия при любом методе лечения рака (например, при лучевой терапии). Хотя это утверждение оказалось верным для ФДТ, представляется перспективной оценка пригодности предложенной модели для других данных.

Ключевые слова: кривые выживаемости клеток, математическое моделирование, фотодинамическая терапия.

Для цитирования: Karami–Gadallo L., Pouladian M. Cancer cell survival model after photodynamic therapy // Biomedical Photonics. – 2022. – Т. 11, № 2. – С. 4–11. doi: 10.24931/2413–9432–2022–11–2–4–11.

Контакты: L. Karami–Gadallo, e-mail: leilakarami271@yahoo.com

Introduction

In order to treat cancer in human, there are different techniques depending on some factors such as type and stage of cancer, specifications of 3D-contour of cancerous tissues (planned tumor volume: PTV), surrounded healthy organs (especially organs at risk: OAR), and cancer distribution from skin toward depth in the diseased organs.

In addition to traditional methods for cancer therapy such as chemotherapy, other techniques might apply photons (from low-frequency electromagnetic waves till x- and gamma-rays), accelerated massy particles (e.g. electrons, neutrons, protons and atoms) and/or mechanical waves (e.g. ultrasound beam). Such rays or beams should transfer energy into the tissues with so characteristics (i.e. spatial/temporal distribution of its intensity) that maximally kill the cancerous cells (through necrosis or apoptosis, mostly) whilst minimally harm surrounding healthy cells. In order to optimize the absorbed energies, a proper treatment plan is required. Different type/energy of any beam/ray has different interactions with the surface to inner tissues leading to different absorbed doses within them. For example, the electron beam is proper for skin and superficial cancers because of its low penetration depth (below a few cm). Although, such beams lead to apoptosis of the cells, unfortunately, generation and applying of them are relatively expensive, complicated and time consuming in addition to their ionization problems for healthy cells.

In contrast, some relatively low cost and accessible techniques are just applying non-ionization waves such as the laser or ultrasound (in the form of high intensity focused) to provide hyperthermia and necrosis in cancerous cells.

Recently, a lot of low power techniques provide some 'killer agents' between cancerous cells using a substance which would be toxic after radiation e.g. photodynamic therapy (PDT).

PDT is a promising treatment modality for cancer therapy using photosensitizer (PS), oxygen and light to destroy malignancy. Photochemical reactions between PS, light and oxygen in the cells leads to production of a cytotoxic agent known as singlet oxygen which could kill the cell. In contrast to chemotherapy and conventional radiotherapy, PDT is known as a minimally invasive technique with selectivity in cancer treatment without any complicated side effects [1-8].

The effectiveness of PDT depends on a large number of parameters including the type and dose of PS, the presenting oxygen level within the cells, the specifications of applied light (including its wavelength and irradiance and also the start/end instants of irradiation after PS incubation) and the optical properties of the tissue at the applied wavelength as well as the type and spreading out of the cancer [9]. In the cases of deep cancers (e.g. head and neck or liver cancer), PDT is performed through optical fibers to reach the light photons to cancerous region [10].

In order to determine the optimized parameters to obtain the most effectiveness of PDT, a variety of experimental and theoretical methods have been suggested by a number of researchers.

In addition to introducing the reliable techniques for PDT dosimetry, our objective in this work was to show the role of the PDT dose in the cell survival through modeling their relation. Some treatment factors (e.g. type and characteristics of drug and light), biological conditions (e.g. cancer type and its distribution) and instrumentation specifications could have main roles in selecting dosimetry method [11]. Some investigators have compared two reported PDT dosimetry techniques through measurement of the $^1O_2$ luminescence or the PS photobleaching fluorescence by which the $^1O_2$ production or the PS consumption respectively could also be tracked during treatment [12]. Some researchers have proposed a microscopic model using the six differential equations (SDE) representing the complex reactions between PS, O_2 molecules, and the emitted photons for producing $^1O_2$ which could react with nucleus receptors leading to apoptosis and cell death [13-14]. Some models quantitating PDT cytotoxicity through showing the relation between survival ratio and different types of killer agents has been introduced by some researchers [15-16]. In one survival model, in addition to the main killer agent [$^1O_2$], the unoxidized receptors concentration (denoted by [R]) was also accounted as the model's inputs [17]. In other words, they added another differential equation showing survival ratio to SDE. Unfortunately, moreover the dependency between these two inputs, [R] could not be obtained practically by measurement. It should be extracted from solving SDE with the inputs of PS concentration, photon density and some variable's initial conditions.

The PDT appears to stimulate several different signaling pathways, some of which lead to cell death, via caspase-dependent and -independent apoptosis whilst some other might cause cell survive depending on biological (e.g. cell type and cell's oxygen magnitude or hypoxia occurrence) and treatment (e.g. structure and concentration of PS, light fluence, and spatial/temporal conditions of PS distribution during irradiation) factors. Additionally, some other factors such as increased repair of induced damage to membrane, to proteins and occasionally to DNA [18], as well as cell cycle phase [19] might also cause resistant to PDT.

Based on these two different cell responses, two pathways with two different resistances against the killer agent could be imagined. Therefore, we would try to make such two-path model for estimation of cell

response with only one practical input representing a reliable killer agent (which could be [$^1O_2$], fluence or irradiation time duration).

Materials and methods

Usually, increasing PDT dose (even till infinite dose) cannot reach the cell living index (e.g. survival ratio or viability) to zero or in other words mostly there is 'non-zero steady state'. It happens because of two possible classes of reasons: measurement error of index and survivor cells.

First class of reason includes common mode factors affecting the index measurement such as background noise and recording (instrumentation) errors. Second class of reasons might correspond to hypoxia occurrence (leading to stopping $^1O_2$ generation); lack of enough PS; the cells far from access of diffused PS and/or photons; and other factors making the killing process unsuccessful (e.g. cell repair mechanisms).

Therefore, it's possible to make all of the cells to be killed under treatment by increasing PDT-dose, especially by applying simultaneously another treatment technique too (e.g. hyperthermia or photon therapy). At first, the survival index with non-zero steady state is analyzed to be modeled.

Model of nonzero steady-state survival index

Since the resistances of the cells against death determine the living index, we could divide the targets (including the cells) under applying killer agent (i.e. PDT dose) in two groups:

1. dose-independent group with constant resistance against the dose variations as shown in Fig. 1 in the form of horizontal line at resistance 40 au (arbitrary unit);

2. sensitive dose-dependent group from infinite resistance at zero dose with an ascending manner toward a residual resistance (e.g. at 20 au in Fig. 1) at infinite dose.

By paying some attentions to the data presenting the relation of index (viability or survival ratio) versus [$^1O_2$] (as PDT-dose or *d*) which obtained *in vitro* studies by a lot of researchers [17,20], it could be seen as a «hyperbolical» curve (i.e. 1/*d*) fitted between logarithm of index versus *d*. Hence, for 'sensitive cells' the relation of resistance R_s could be considered as the form of below:

$$R_s = R_\infty . e^{1/(s.d)} \quad (1)$$

In which the parameter of R_∞ is the resistance of sensitive cells at infinite *d* and *s* shows the sensitivity (in Fig. 1, *s* is 0.25 for more and 0.07 for less sensitive curves; R_∞ is 20 for both).

Two resistances of non-sensitive R_{ns} (i.e. constant R_0) and sensitive R_s (i.e. Eq. 1) act in parallel to make the total resistance of all cells as $(R_s*R_{ns})/(R_s+R_{ns})$ which simplified in the form of

$R_0/[1+(R_0/R_\infty)*\exp(-1/s*d)]$ appeared as a mirrored (right-to-left) "S"-shaped (i.e. mirrored sigmoidal).

Finally, we could present our model in the following equation to quantitate the PDT response "with nonzero steady state" (i.e. nonzero *v* at infinite *d*) as the variable v versus *d* as:

$$v(d) = \frac{v_0}{1 + m\ .e^{-1/s.d}} \quad (2)$$

where *v(d)* can be interpreted as either the cell viability, the survival index, the numbers of cells, or the probability of cell survival with setting relevant (positive) value of parameters v_0 (i.e. 100 or 1), *m*, and *s* for each one. In Fig. 2, the effect of *m* variation on the steady state (up) and *s* variation on the slope or sensitivity (down) could be seen for mirrored-sigmoid curve of Eq.2.

The parameters Concepts of the Model

In Eq. 2, the parameter v_0 means the magnitude of *v* at *d* equals to 0 (usually v_0 is 100 or 1), whilst at 'steady state' $d=\infty$ it is $v_\infty = v_0/(1+m)$. Hence, the parameter *m* could be calculated based on the initial condition v_0 and the final condition v_∞ (if presented) as follows:

$$m = (v_0 - v_\infty)/v_\infty \quad (3)$$

The parameter *s* shows the slope of descending part of mirrored sigmoid curve and relates to sensitivity.

It could be obtained by setting *d* at value 1/*s* (in Eq.2) at which *v* reaches to 1/(1+*m*/*e*) of its initial (v_0) as follows:

$$V\left(at\ d = s^{-1}\right) = \frac{V_0}{1 + me^{-1}} \quad (4)$$

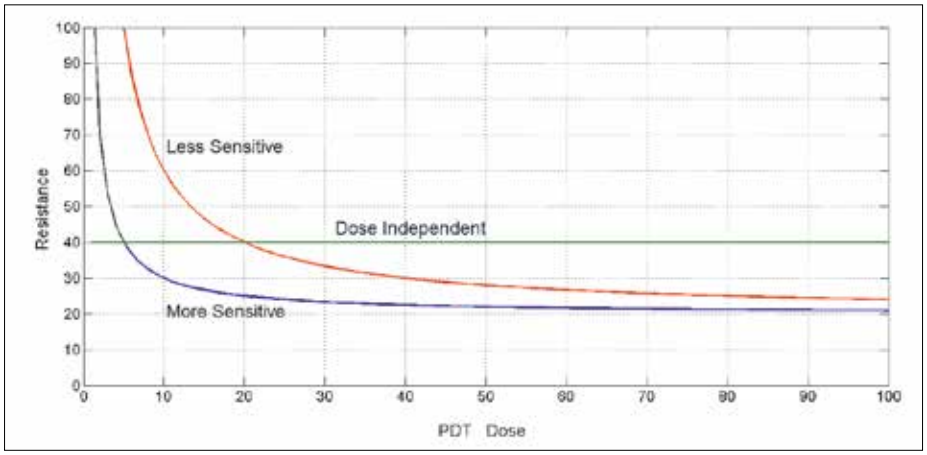

Рис. 1. Два типа устойчивости клеток при изменении параметров ФДТ: дозозависимая (два типичных случая с высокой и низкой чувствительностью) и постоянная устойчивость (нечувствительная). Оси имеют произвольные единицы измерения (усл.ед.).

Fig. 1. Two types resistances of the cells against PDT-Dose variations: dose-dependent (two typical cases with high and low sensitivity) and constant resistance (non-sensitive). The axes have arbitrary units (au).

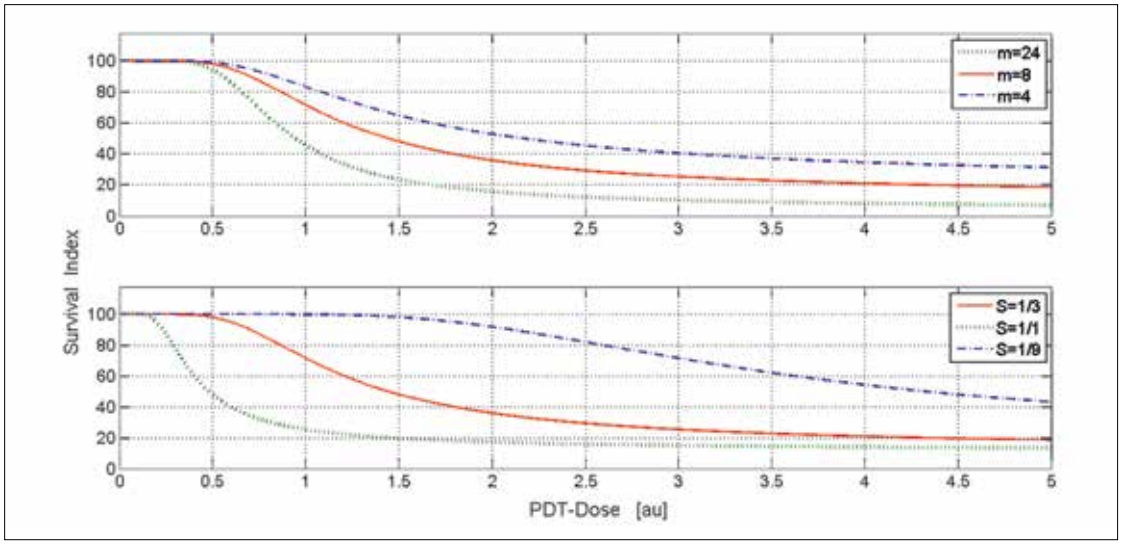

Рис. 2. Образцы зеркально-сигмовидной формы (дозы в усл.ед.) для V_0=100 и измененных двух параметров: (вверху) различные m для s=1/3; (внизу) различные s для m=8.

Fig. 2. Samples of mirrored sigmoid-shaped (with arbitrary units of the dose) for V_0=100 and altered two parameters: (Up) different m for s=1/3; (Down) different s for m=8.

One of the important points of such curves is the critical point (CP) d_c at where the curve appears linear (around d_c) with the most descending slope; and the second derivative of *v* becomes zero (i.e. $\frac{\partial^2 V}{\partial D^2}=0$ at $d=d_c$).

Therefore it could be found a relation between *Dc, m,* and *S* as follows:

$$s=\frac{1-me^{-1/(s.d_c)}}{2d_c(1+me^{-1/(s.d_c)}} \quad (5)$$

It could be shown that according to Eq.5, one could write down:

$$if\ m \ll e^2\ then\ s=1/(2d_c)$$
$$if\ m>1 then\ s<(d_c.log\ m)^{-1} \quad (6)$$

Model of Zero Steady-State Survival Index

If any cell killing-factor was added to a treatment process (e.g. adding a second therapy technique), residual sensitive cells initiated to decrease their resistance against death (i.e. decreasing R_∞) so that Rs trends to zero at high doses (i.e. steady state). Hence, Eq. 1 could be enhanced by multiplying the parameter R_∞ to an exponent term (i.e., $e^{s_2 d}$) in order to increase decaying the steady state. After affecting non-sensitive parallel resistance and some simplifications, survival index became as:

$$v(d)=\frac{v_0}{1+me^{S_2 d-1/(S_1 d)}} \quad (7)$$

that could be applied with related initial condition v_0 (*v* at zero *d*) and three parameters *m*, s_1 and s_2. By setting s_2 to zero the Eq. 7 converts to Eq. 2.

Data Acquisition

In order to validate the final model, type-II PDT data extracted from other (in vitro) work [20] was applied. The drug of 5-AminoLevulinic Acid (ALA; from 'Sigma Chemical Co') was dissolved in distilled water to obtain the stock solution (1mg/ml). After applying ALA-PDT for some 15-samples groups and providing a control group, the cell viabilities were obtained for different irradiated times for model validation.

Cell Culture

The human lung carcinoma cell (A-549) was supplied by Iranian Biological Resource Center and cultured in DMEM: Ham'SF12 + 2Mml-Glutamine+ 10% FBS in a 5% CO2 incubator at 37^{0C}. A549 cell lines were seeded into 96-well plates at concentration of 1×10^4 cells per well and were incubated for 24 hours for proper attachment to substratum. After 70–75% cell confluence, the media of wells was removed then phosphate buffered saline and 10µl 5-ALA per well added to them and incubated for 3 h.

ALA-PDT

Except the control (no ALA; no light) and ALA groups, others were irradiated with LED light (632 nm at a fixed flounce rate 35mw/cm^2) for different time durations (till 300 seconds). We repeated the test for another ALA administration too in order to obtaining 5 and 10 µl 5-ALA per well.

MTT Assay

At 24 h after the treatment, cell viabilities were obtained through MTT evaluation method using an optical densitometry technique at 570 nm measuring the activity of mitochondria and cellular dehydrogenase enzymes. The data were analyzed by one-way ANOVA statistical method in SPSS software.

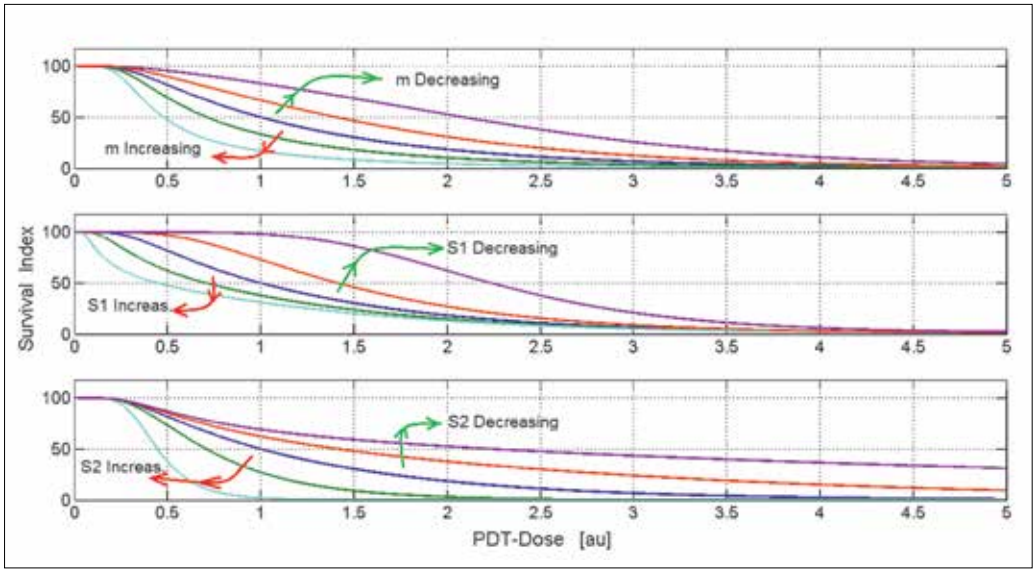

Рис. 3. Отклонения формы модели сигмоидальной кривой при значениях 1/5, 1/2, 2 и 5 для параметров m (вверху), s_1 (посередине), s_2 (внизу) относительно центральной кривая в качестве контроля с m=1, s_1=1 и s_2=1.
Fig. 3. Shape deviations of the sigmoidal-curve model for the values of 1/5, 1/2, 2, and 5 for the parameters: m (top), s_1 (middle), and s_2 (bottom) relative to central curve as the control with m=1, s_1=1, and s_2=1.

Results

We proposed a model (as shown in Eq. 7) to obtain the cell survival index (that could be cell viability, survival probability, or any index representing cell living conditions) as a function of PDT-dose (that could be illuminating time, fluence, $[^1O_2]$ or any variable representing the killer agent dose).

When experimental findings show a number of points in dose-v plane, one could extract approximately some specifications (such as the location of CP and its slope, shoulder/plateau width, vanishing speed, and the steady state magnitude) to find the model's parameters roughly.

Moreover, one could easily fit the best sigmoid-curve with the data by different mathematical techniques (found in the curve fitting toolkit of MatLab software) to obtain the optimized parameters (with minimum root mean squared error-RMSE).

In order to understand the effects of the parameters alterations on the shape of model, different magnitudes of *m*, s_1 and s_2 were applied (v_0=100) and the results compared with a control curve appeared in the central of curves in Fig. 3.

As seen in Fig. 3, the parameters could control curve features as follows:

top: *m* could control CP's slope and the ascending window width, whilst maintain approximately CP's location;

middle: s_1 could control CP's location, whilst maintain approximately its slope, hence control the plateau width,;

bottom: s_2 could control CP's slope, whilst maintain approximately its location and also the ascending window width, hence control the steady state magnitude.

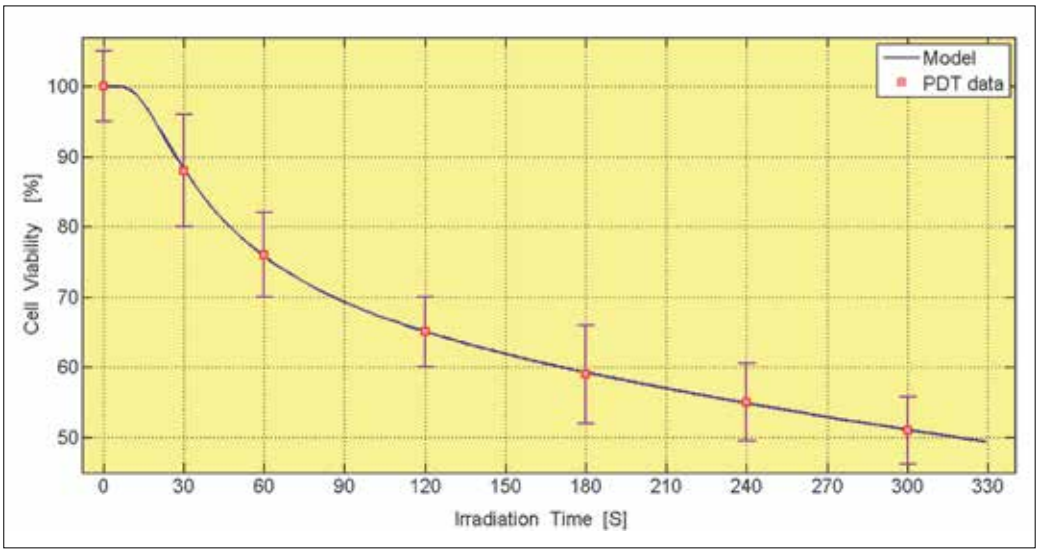

Рис. 4. Данные АЛК-ФДТ и выходные данные модели (с m = 0,6444, s_1 = 0,02052, s_2 = 0,001863)
Fig. 4. The ALA-PDT data and the model output (with m=0.6444, s_1=0.02052, s_2=0.001863)

As shown in Fig. 4, the model was validated using the obtained ALA-PDT data showing an excellent fitting relative to other models (such as single/multi target/hit inactivation, two components and linear quadratic models).

Furthermore, based on our findings, ALA did not produce considerable dark toxicity at any concentration or incubation time as verified by the MTT assay. It was found that increasing the irradiation time make the cell survival to be decreased. These findings are consistent with different ALA doses used in similar studies with other cell lines [1,3,16]. The cell death of 90% was seen (for 10 µl ALA per well) for the irradiation time of about 21 min (i.e. 24 min by the model) whilst at about 300 s (i.e. 320 s by the model) the lethal dose 50% (known as LD_{50}) observed.

By repeating the test for half ALA concentration (i.e. 5 µl per well; not shown in Fig. 4), the findings didn't vary significantly for low doses whilst a little difference for high doses (e.g. LD_{50} appeared at about 7 min) was seen.

Discussion

The PDT is a promising modality and clinically approved for treatment of certain tumors and several types of neoplasms including cutaneous lesions, non-small cell lung carcinomas, head/neck and esophageal cancers [1-8,10,21]. In PDT researches, presenting multifactorial and complex photochemical processes (e.g. multi molecular interaction, spatial/temporal variation of the concentration before and during the irradiation time) could cause challenging problems in the analysis and dosimetry of PDT and hence limit the related studies variety.

This study was designed firstly to determine the effect of varying the ALA-mediated PDT dose (i.e. different flounce; or irradiation time here) on the survival of non-small cells of lung carcinoma (in vitro) and secondly to model mathematically their relation.

It could be noticed that the relation curve between the cell survival and the killer agent in all of the cancer treatment methods (even including radiotherapy) has a mirrored sigmoidal form such as radiobiological models (e.g. m-hits n-targets or linear quadratic models) [22].

However, it could be imagined that for any survival curve there are approximately three ideal main regions: the plateau (negligible effect; a bit cell death at low doses), the descending slope (the most sensitivity; the most killing rate at the critical dose) and the steady state segment as shown in Fig. 5.

In Eq.7, the survival index *v* could be approximately (assuming error under 10%) equivalent to $1/[1+m*\exp(-1/(s_1*d)]$ for low doses (i.e., $d < 1/(10*s_2)$, and $1/[1+m*\exp(s_2*d)]$ for high doses ($d > 10/s_1$). Hence, these three geometric features (as shown in Fig. 5) could be determined through three parameters of the model (as could be noticed in Fig. 2). Nonetheless, the features could be visualized to have some proportional relations with the most affectivity parameters as follows:

$$s_1 \downarrow \Rightarrow plateau\ width \uparrow$$

$$m \uparrow or\ s_2 \uparrow \Rightarrow slope \uparrow \quad (\text{if } d > 1/m \text{ then } s_2 \text{ is more affective else, } m \text{ is})$$

$$m \downarrow or\ s_2 \downarrow \Rightarrow tail\ height \uparrow \quad (\text{if } d > 1/m \text{ then } s_2 \text{ is more affective else, } m \text{ is}) \quad (7)$$

Hence, from biological viewpoint, the sensitivity parameters (i.e., s_1 and s_2) and the sensitivity magnifier parameter (i.e., *m*) could be mostly interpreted as follows:

The 'cell killing dose threshold' could be controlled mostly by s_1; whilst the 'cell killing velocity' by s_2 and the 'steady-state survived cells' by *m*.

Also, from biochemical viewpoint, it could be said: the more affective and proper of PS, the more s_2 value; the more diehard and resistant of the cells against killer agent, the less s_1; the more concentration of PS and oxygen, the more *m* value.

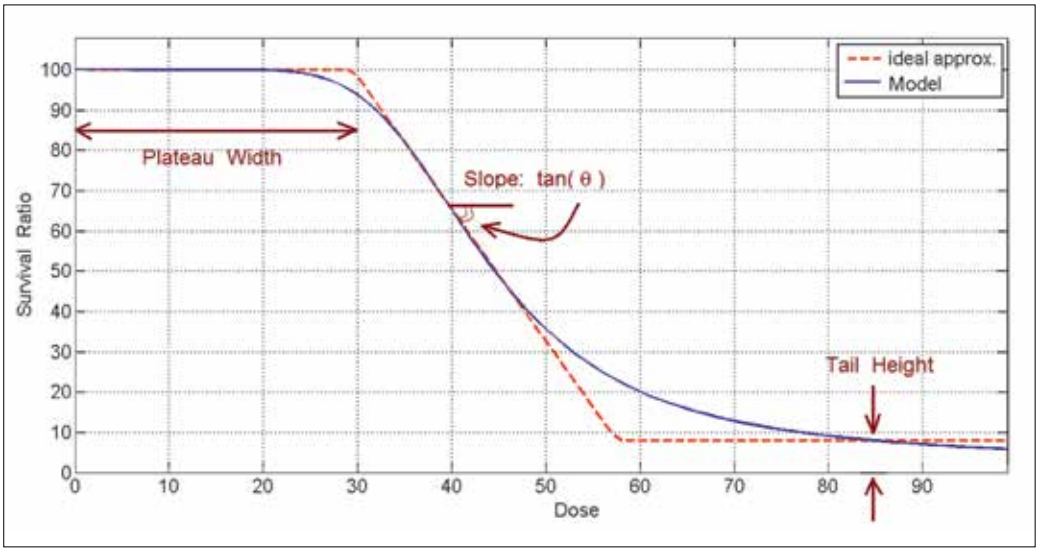

Рис. 5. Пример модели (с параметрами: m=491, s_1=0,00385, s_2=0)
Fig. 5. A sample of the model (with parameters: m=491, s_1=0.00385, s_2=0).

However, accurate biological interpretation of our model's parameters is still unknown as well as other model's ones.

From the mathematical view (i.e. MSER), our model could fit better than other models (e.g., target-theory based models [23]) on the obtained PDT-data (MSER findings were not presented here).

If a treatment technique could not kill all of the cancerous cells (i.e. constant steady sate), the model of Eq.2 (or Eq.7 with s_2=0) might be applied with two parameters (as follows: *m* depending on the requirements of the technique (e.g., PS and oxygen concentrations) and target conditions (e.g., the population rate of non-sensitive cells); and *s* depending on the effectiveness of the killer agent (i.e. the sensitivity). According to Fig. 5, it could be said that the more *m*, the less tail height whilst the more s, the more slope and the less plateau width. If a second treatment technique is also applied simultaneously, one might use its sensitivity as s_2 in the model Eq.7.

The presented model could show a plateau or shoulder on the cell survival curve whose size could be varied by the model parameters (i.e. mostly s_1) based on the technique performance in low doses. Moreover, in contrast to other models (including two compartment and/or linear quadratic ones), the curve maintains its sigmoid shape even in logarithmic scales (not shown in figures here) which is consistent with experiments.

In order to modeling of the viability, survival probability, and the population of the cells, v_0 in Eq.7 should be set respectively to 100, 1, and the cells initial number.

By using a radioisotope in 'for example gamma camera', a variable presenting cellular metabolism could be obtained from an image of cancerous region. On the other hand, the absorbed dose of related killer agent (e.g. x-ray or electron-beam) could also be measured by relevant dosimetry technique. Hence, obtaining the metabolism level versus different treatment doses could provide some data in the form of various points in the dose-metabolism plane.

It seems model of Eq.7 could fit a proper curve on such data better than other models [22] could. «Encompassing the most fitness on real cellular response to any killer agent» for our model is the statement that we are working on its validity.

Conclusion

A mathematical model (with three parameters m, S_1, and S_2) was proposed which seems to be fitted better than other models on the cell survival data versus the killer agent dose. Here, it was tested for the cell viability data versus different irradiation time durations in ALA-PDT (on the lung cancerous cells in vitro) resulting excellent fitting. The mirrored (right-to-left) sigmoid curve generated from this model had a shoulder as usually needed for mammalian survival curve; moreover, this curve kept its nonlinear-shape in semi-logarithmic scale. By tuning three parameters of the model, it could make any required form in the survival curve for both regions of low doses (slow variations) and high doses (steady-state) as well as the descending part (which is linear about the steepest point). However, it is needed to test this model by the survival data of any cancer-therapy technique applied by other researchers. It is also essential to consider the correlations between the model's parameters and treatment factors in order to obtain the best biological interpretations for the parameters.

Acknowledgement

The authors would like to thank Sama Pouladian for her help in providing figures. This research did not receive any specific grant from funding agencies in the public-commercial, or non-for-profit sectors.

REFERENCES

1. Girotti A. Photodynamic Therapy of Neoplastic Disease, *CRC Press*, Boca Raton, FL, USA: 1990.
2. Filonenko E.V. Clinical implementation and scientific development of photodynamic therapy in Russia in 2010-2020, *Biomedical Photonics*, 2021, vol. 10, no. 4, pp. 4–22. doi: 10.24931/2413–9432–2021–9-4-4-22
3. Sokolov V.V., Filonenko E.V., Telegina L.V. et al. Combination of fluorescence imaging and local spectrophotometry in fluorescence diagnostics of early cancer of larynx and bronchi, *Quantum Electronics*, 2002, vol. 32, no. 11, pp. 963–969. doi: 10.1070/QE2002v032n11ABEH002329
4. Agostinis P. et al. Photodynamic therapy of cancer: an update, *CA Cancer J. Clin*., 2011, vol. 61 (4), pp. 250–281.
5. Filonenko E.V., Kaprin A.D., Raszhivina A.A., Urlova A.N., Nechipai A.M. Fluorescence diagnostics of colon

ЛИТЕРАТУРА

1. Girotti A. Photodynamic Therapy of Neoplastic Disease // CRC Press; Boca Raton, FL, USA: 1990.
2. Filonenko E.V. Clinical implementation and scientific development of photodynamic therapy in Russia in 2010-2020 // Biomedical Photonics. – 2021. – Т. 10, № 4. – С. 4–22. doi: 10.24931/2413-9432-2021-9-4-4-22
3. Sokolov V.V., Filonenko E.V., Telegina L.V., Boulgakova N.N., Smirnov V.V. Combination of fluorescence imaging and local spectrophotometry in fluorescence diagnostics of early cancer of larynx and bronchi // Quantum Electronics. – 2002. – Vol. 32(11). – P. 963–969. doi: 10.1070/QE2002v032n11ABEH002329
4. Agostinis P. et al. Photodynamic therapy of cancer: an update // CA Cancer J. Clin. – 2004. Vol. 61 (4) – P. 250–281.
5. Filonenko, E.V., Kaprin, A.D., Raszhivina, A.A., Urlova, A.N., Nechipai, A.M. Fluorescence diagnostics of colon malignant and premalignant

malignant and premalignant lesions using 5-aminolevulinic acid, *International Journal of Photoenergy*, 2014, no. 378673. doi: 10.1155/2014/378673
6. Filonenko E.V., Ivanova-Radkevich V.I. Photodynamic therapy in the treatment of patients with mycosis fungoides, *Biomedical Photonics*, 2022, vol. 11, no. 1, pp. 27–36. doi: 10.24931/2413–9432–2022–11-1-27-36.
7. Henderson B.W., Dougherty T.J. How does photodynamic therapy work? *Photochem. Photobiol.*, 1992, vol. 55, pp. 145–157.
8. Filonenko E.V. The history of development of fluorescence diagnosis and photodynamic therapy and their capabilities in oncology, *Russian Journal of General Chemistry*, 2015, vol. 85(1), pp. 211–216. doi: 10.1134/S1070363215010399
9. Helander L., Krokan H.E., Johnsson A., Gederaas O.A., Plaetzer K. Red versus blue light illumination in hexyl 5-aminolevulinate photodynamic therapy: the influence of light color and irradiance on the treatment outcome in vitro, *Journal of Biomedical Optics*, 2014, vol. 19(8), pp. 088002.
10. Jerjes W., Upile T., Betz C.S., El Maaytah M., Abbas S., Wright A. et al. The application of photodynamic therapy in the head and neck, *Dent Update*, 2017, vol. 34, pp. 478-486.
11. Zheng Huang et al. Photodynamic therapy for treatment of solid tumors – potential and technical challenges, *Technol Cancer Res Treat*, 2008, vol. 7(4), pp. 309–320.
12. Jarvi M.T., Patterson M.S., Wilson B.C. Insights into Photodynamic Therapy Dosimetry: Simultaneous Singlet Oxygen Luminescence and Photosensitizer Photobleaching Measurements, *Biophysical Journal Volume*, 2012, vol. 102, pp. 661–671.
13. Foster, T.H., Murant R.S., Bryant R.G., Knox R.S., Gibson S. L. and Hilf R. Oxygen consumption and diffusion effects in photodynamic therapy, *Radiat. Res.*, 1991, vol. 126, pp. 296–303.
14. Valentine R.M., Ibbotson S.H., Wood K., Brown C.T. Modelling fluorescence in clinical photodynamic therapy, *Photochem Photobiol Sci*, 2013, vol. 12(1), pp. 203–13 [PubMed: 23128146]
15. Pelicano H., Carney D. and Huang P. ROS stress in cancer cells and therapeutic implications, *Drug Resist. Updat.*, 2014, vol. 7, pp. 97–110.
16. Belousova I. M., Mironova N.G. and Yur'ev M.S. A mathematical model of the photodynamic fullerene-oxygen action on biological tissues, *Opt. Spectrosc*, 2015, vol. 98, pp. 349–356.
17. Ioannis Gkigkitzis, Yuanming Feng, Chunmei Yang, Jun Q. Lu and Xin-Hua Hu. Modeling of Oxygen Transport and Cell Killing in Type-II Photodynamic Therapy, *Photochemistry and Photobiology*, 2012, vol. 88, pp. 969–977.
18. Casasa A., Di Venosa G., Hasan T. and Batllea A. Mechanisms of Resistance to Photodynamic Therapy, *Curr Med Chem*, 2011, vol. 18(16), pp. 2486–2515.
19. Wyld L., Smith O., Lawry J., Reed M.W. and Brown N.J. Cell cycle phase influences tumour cell sensitivity to aminolaevulinic acid-induced photodynamic therapy in vitro, *Br J Cancer*, 1998, vol. 78(1), pp. 50–55.
20. Karami Gadallo L., Ghoranneviss M., Ataie-Fashtami L., Pouladian M., Sardari D., Enhancement of Cancerous Cells Treatment by Applying Cold Atmosphere Plasma and Photo Dynamic Therapy Simultaneously, *Clinical Plasma Medicine*, 2017 http://dx.doi.org/10.1016/j.cpme.2017.08.002
21. Chen X., Zhao P., Chen F., Li L., and Luo R. Effect and mechanism of 5-aminolevulinic acid-mediated photodynamic therapy in esophageal cancer, *Lasers Med Sci*, 2011, vol. 26, pp. 69-78.
22. Bodgi L. et al. Mathematical models of radiation action on living cells: From the target theory to the modern approaches. A historical and critical review, *Journal of Theoretical Biology*, 2011, vol. 394, pp. 93 –101.
23. Nomiya T. Discussions on target theory: past and present, *J Radiat Res*, 2013, vol. 54(6), pp. 1161–1163.

lesions using 5-aminolevulinic acid // International Journal of Photoenergy. – 2014. – № 378673 Doi: 10.1155/2014/378673
6. Filonenko E.V., Ivanova-Radkevich V.I. Photodynamic therapy in the treatment of patients with mycosis fungoides // Biomedical Photonics. – 2022. – T. 11, № 1. – C. 27–36. doi: 10.24931/2413–9432–2022–11-1-27-36.
7. Henderson B.W., Dougherty T.J. How does photodynamic therapy work? // Photochem. Photobiol. – 1992. – Vol. 55. – P. 145–157.
8. Filonenko E.V. The history of development of fluorescence diagnosis and photodynamic therapy and their capabilities in oncology // Russian Journal of General Chemistry. – 2015. – Vol. 85(1). – P. 211–216. doi: 10.1134/S1070363215010399
9. Helander L., Krokan H.E., Johnsson A., Gederaas O.A., Plaetzer K. Red versus blue light illumination in hexyl 5-aminolevulinate photodynamic therapy: the influence of light color and irradiance on the treatment outcome in vitro // Journal of Biomedical Optics. – 2014. – Vol. 19(8). – P. 088002.
10. Jerjes W., Upile T., Betz C.S., El Maaytah M., Abbas S., Wright A. et al. The application of photodynamic therapy in the head and neck // Dent Update. 2017. – Vol. 34. – P. 478-486.
11. Zheng Huang et al. Photodynamic therapy for treatment of solid tumors – potential and technical challenges // Technol Cancer Res Treat. – 2008. – Vol. 7(4). – P. 309–320.
12. Jarvi M.T., Patterson M.S., Wilson B.C. Insights into Photodynamic Therapy Dosimetry: Simultaneous Singlet Oxygen Luminescence and Photosensitizer Photobleaching Measurements // Biophysical Journal Volume. – 2012. – Vol. 102. – P. 661–671.
13. Foster, T.H., Murant R.S., Bryant R.G., Knox R.S., Gibson S. L. and Hilf R. Oxygen consumption and diffusion effects in photodynamic therapy // Radiat. Res. – 1991. – Vol. 126. – P. 296–303.
14. Valentine R.M., Ibbotson S.H., Wood K., Brown C.T. Modelling fluorescence in clinical photodynamic therapy // Photochem Photobiol Sci. – 2013. – Vol. 12(1). – P. 203–13 [PubMed: 23128146]
15. Pelicano H., Carney D. and Huang P. ROS stress in cancer cells and therapeutic implications // Drug Resist. Updat. – 2014. – Vol. 7. – P. 97–110.
16. Belousova I. M., Mironova N.G. and Yur'ev M.S. A mathematical model of the photodynamic fullerene-oxygen action on biological tissues // Opt. Spectrosc. – 2015. –Vol. 98. – P. 349–356.
17. Ioannis Gkigkitzis, Yuanming Feng, Chunmei Yang, Jun Q. Lu and Xin-Hua Hu. Modeling of Oxygen Transport and Cell Killing in Type-II Photodynamic Therapy // Photochemistry and Photobiology. – 2012. – Vol. 88. – P. 969–977.
18. Casasa A., Di Venosa G., Hasan T. and Batllea A. Mechanisms of Resistance to Photodynamic Therapy // Curr Med Chem. – 2011. – Vol. 18(16). – P. 2486–2515.
19. Wyld L., Smith O., Lawry J., Reed M.W. and Brown N.J. Cell cycle phase influences tumour cell sensitivity to aminolaevulinic acid-induced photodynamic therapy in vitro // Br J Cancer. 1998. – Vol. 78(1). – P. 50–55.
20. Karami Gadallo L., Ghoranneviss M., Ataie-Fashtami L., Pouladian M., Sardari D., Enhancement of Cancerous Cells Treatment by Applying Cold Atmosphere Plasma and Photo Dynamic Therapy Simultaneously // Clinical Plasma Medicine. – 2017. http://dx.doi.org/10.1016/j.cpme.2017.08.002
21. Chen X., Zhao P., Chen F., Li L., and Luo R. Effect and mechanism of 5-aminolevulinic acid-mediated photodynamic therapy in esophageal cancer // Lasers Med Sci. – 2011. –Vol. 26. – P. 69-78.
22. Bodgi L. et al. Mathematical models of radiation action on living cells: From the target theory to the modern approaches. A historical and critical review // Journal of Theoretical Biology. – 2011. – Vol. 394. – P. 93 –101.
23. Nomiya T. Discussions on target theory: past and present // J Radiat Res. – 2013. – Vol. 54(6). – P. 1161–1163.

ORIGINAL ARTICLES

APPLICATION OF BIOPHANTOMES TO EVALUATE THE THERMAL EFFECTS OF LASER RADIATION WITH WAVELENGTHS OF 970 NM AND 1560 NM UNDER DIFFERENT EXPOSURE MODES

Ostreiko O.V., Galkin M.A., Papayan G.V., Grishacheva T.G., Petrishchev N.N.
Pavlov First Saint-Petersburg State Medical University, Saint-Petersburg, Russia

Abstract

Laser interstitial hyperthermia is an actively developing direction in intracerebral tumor surgery. The paper presents thermal effects in polyacrylamide biophantoms with bovine albumin and citrated blood under laser irradiation at 970 nm and 1560 nm. For laser irradiation, a surgical two-wave apparatus manufactured by IRE Polis was used. The phantom was irradiated through a quartz optical fiber 400 μm in diameter with an end exit. The result of irradiation of the phantom was its coagulation zone, which was visualized with a FLUM-LL fluorescent organoscope. Thermometry was carried out with a FLIRONE PRO for IOS thermal imager and a T-8 digital thermograph based on a laptop with thermal sensors placed in a phantom. The use of irradiation with a power of not more than 2 W in the coagulation mode, with a total energy dose of up to 120 J, made it possible to achieve a smooth rise in temperature to 88.0 °C. The dimensions of the coagulation zone under irradiation with a wave of 1560 nm were always larger than under irradiation with a wave of 970 nm, although the difference was not statistically significant (p=0,41). Thus, the average coagulation spot area for 970 nm radiation was 43.2 (39.3 – 47.1) mm^2, and for 1560 nm – 99.4 (56.5-141.3) mm^2. With total irradiation with two waves, the coagulation zone was larger if the radiation power of 1560 nm prevailed. When irradiated with a wave of 970 nm, the coagulation zone partially propagates posteriorly from the tip of the optical fiber, and 1560 nm coagulates the phantom anteriorly. The results obtained are of practical importance for laser hyperthermia of intracerebral tumors.

Key words: biophantom, biophantom laser irradiation thermometry, laser hyperthermia of intracerebral tumors, hyperthermia modes.

For citation: Ostreiko O.V., Galkin M.A., Papayan G.V., Grishacheva T.G., Petrishchev N.N. Application of biophantomes to evaluate the thermal effects of laser radiation with wavelengths of 970 nm and 1560 nm under different exposure modes, *Biomedical Photonics*, 2022, vol. 11, no. 2, pp. 12–22.doi: 10.24931/2413–9432–2022–11-2-12-22.

Contacts: Ostreiko O.V., e-mail: oleg.v.ostreiko@mail.ru

ПРИМЕНЕНИЕ БИОФАНТОМОВ ДЛЯ ОЦЕНКИ ТЕРМИЧЕСКИХ ЭФФЕКТОВ ЛАЗЕРНОГО ИЗЛУЧЕНИЯ С ДЛИНАМИ ВОЛН 970 НМ И 1560 НМ ПРИ РАЗНЫХ РЕЖИМАХ ВОЗДЕЙСТВИЯ

О.В. Острейко, М.А. Галкин, Г.В. Папаян, Т.Г. Гришачева, Н.Н. Петрищев
Первый Санкт-Петербургский государственный медицинский университет
им. акад. И.П. Павлова, Санкт-Петербург, Россия

Резюме

Лазерная интерстициальная гипертермия – активно развивающееся направление в хирургии внутримозговых опухолей. В работе представлены термические эффекты в полиакриламидных биофантомах с бычьим альбумином и цитратной кровью при лазерном облучении на длине волны 970 нм и 1560 нм. Для лазерного облучения использован хирургический двухволновый аппарат (ИРЭ «Полис», г. Фрязино, Россия). Облучение фантома осуществлялось через кварцевое световолокно диаметром 400 мкм с торцевым выходом. Результатом облучения была зона коагуляции, которая визуализирована флуоресцентным органоскопом «FLUM-LL». Термометрия осуществлялась тепловизором FLIRONE PRO for IOS и цифровым термографом Т-8 на базе ноутбука с термосенсорами, размещенными в фантоме. Использование облучения мощностью не более 2 Вт в режиме коагуляции с суммарной дозой энергии до 120 Дж позволяло достигать плавного подъема температуры до 88°С. Зона коагуляции при облучении волной 1560 нм всегда

была больше, чем при облучении волной 970 нм, хотя статистически разница была недостоверной (p=0,41). Средняя площадь пятна коагуляции для излучения 970 нм составила 43,2 (39,3 – 47,1) мм^2, для 1560 нм – 99,4 (56,5 – 141,3) мм^2. При суммарном облучении двумя волнами, зона коагуляции была больше, если преобладала мощность излучения 1560 нм. При облучении волной 970 нм зона коагуляция частично распространяется кзади от кончика световолокна, при 1560 нм – коагулирует фантом кпереди. Полученные результаты имеют практическую значимость при применении лазерной гипертермии внутримозговых опухолей.

Ключевые слова: биофантом, термометрия лазерного облучения биофантома, лазерная гипертермия внутримозговых опухолей, режимы гипертермии.

Для цитирования: Острейко О.В., Галкин М.А., Папаян Г.В., Гришачева Т.Г., Петрищев Н.Н. Применение биофантомов для оценки термических эффектов лазерного излучения с длинами волн 970 нм и 1560 нм при разных режимах воздействия // Biomedical Photonics. – 2022. – Т. 11, № 2. – С. 12–22. doi: 10.24931/2413–9432–2022–11-2-12-22.

Контакты: Острейко О.В., e-mail: oleg.v.ostreiko@mail.ru

Introduction

Standard treatments for brain tumors include surgery, radiation therapy, and chemotherapy. Despite an integrated approach to the treatment of malignant glial tumors, the prognosis remains unfavorable. Since surgical treatment is critical, it is necessary to develop effective and less invasive cytoreductive surgical techniques that do not cause damage to healthy tissues. Over the past 30 years, research has been carried out on hyperthermic procedures as an alternative to classical open operations [1–3]. Interstitial hyperthermia of brain tumors under the influence of infrared laser radiation is a less invasive and safer technique than traditional surgical technologies.

Understanding the interaction of laser radiation with tumor tissue and its prediction underlie the development and improvement of laser hyperthermia methods [4]. The wavelength is the fundamental characteristic of laser light, which determines the tissue effects in the irradiated tumor. This is due to the strong dependence of the interaction with the main absorbent molecules in the brain tumor tissue – water and hemoglobin. With this in mind, radiation characteristics are selected, such as power, exposure, power density, and temporal characteristics of radiation. Clinical application of laser thermal destruction in surgery of brain tumors is implemented by the LITT (laser interstitial thermotherapy) method, its purpose is coagulation of tumor tissue controlled by magnetic resonance thermometry [5, 6]. To implement the technology, two Visualase Thermal Therapy System (Medtronic Inc.) and NeuroBlate System (Monteris Medical, Inc.) are currently produced (or commercially available). They use only two wavelengths of laser radiation: 970 nm and 1064 nm, which have similar characteristics of interaction with the tissue, due to the good absorption of these wavelengths by hemoglobin, which provides a hemostatic effect. At The Pavlov First Saint Petersburg State Medical University an original minimally invasive technique for interstitial laser hyperthermia of glial tumors was developed [7]. From a clinical point of view, the use of other wavelengths that have different effects on biological tissue, but are also suitable for interstitial thermal destruction of tumors is of interest.

An important role in the study of thermal effects arising from laser irradiation of biological tissues is played by biophantoms, which have analogous characteristics of thermal conductivity, heat capacity, and heat transfer rate. As close as possible in composition and optical properties to the tissue under study, they allow you to quickly test and visually observe the effects of laser exposure, carried out using different wavelengths in real time. At the same time, despite the absence of microcirculation in biophantoms, it seems possible to study the main characteristics of biological effects (ablation, coagulation, evaporation, carbonization) and the temperature dependence in the hyperthermia zone on the selected wavelength.

To solve research problems, the phantom must contain a pigment that effectively absorbs laser radiation in the required range. As such a pigment, for example, hemoglobin, Chinese ink or Kromagen Magenta MB60-NH concentrate are used. In addition, for the visual assessment of damage caused by the laser, it is important that the phantom is made of transparent material. One way to determine the temperature gradient in a phantom is to introduce thermochromic dyes that change shades depending on the temperature. The introduction of proteins, such as bovine serum albumin (BSA) or hen's egg protein, into the biophantom makes it possible to observe thermal denaturation of the protein, which is noticeable due to clouding of the transparent medium [8-11].

The most popular materials used as the basis for phantoms are agar and polyacrylamide [9, 11, 12]. Polyacrylamide gels are synthesized by the copolymerization of acrylamide and methylenebisacrylamide in an

aqueous solution. Such a gel is transparent and allows visualization and measurement of heat-affected zones. In addition, polyacrylamide itself is a non-toxic, highly stable and biocompatible polymer. For example, N-isopropylacrylamide gel (NIPAM) becomes cloudy when heated to a certain temperature, which can be changed by varying the concentration of acrylic acid. Gels based on NIPAM have acoustic and thermal characteristics close to those of various biological tissues. It is important to note that these gels can be used multiple times. Whereas in a polyacrylamide gel with BSA, thermal treatment leads to irreversible protein denaturation, in the case of NIPAM, the cloudiness caused by heating gradually disappears upon cooling, and the phantom can be used again [13].

The use of phantoms that are as close as possible in terms of the content of chromophores and optical properties makes it possible to conduct test studies, visually observe the effects of laser exposure, measure temperature in real time, describe and predict the propagation of light energy in tissues.

Materials and methods

In the study of the effect of laser radiation on the biophantom, we used two wavelengths: traditional – 970 nm and 1560 nm. Radiation with a wavelength of 970 nm mainly absorbs hemoglobin, 1560 nm – water, including that contained in whole blood (Fig. 1). Such multidirectional interaction with the main chromophores is of practical interest when using laser coagulation of tumors, since it is due to the heterogeneity of the morphological and biological characteristics of neoplasms, including edema, the number of vessels, and cell density in neoplasms of various histological structures and grades of malignancy. In this case, the absorption of laser radiation and the subsequent release of heat in certain areas of the tissue are the key effects in laser hyperthermia of tumors.

When selecting the material for optical phantoms, we took into account both their mechanical properties, such as elasticity, and thermal characteristics. Based on the combination of these properties, the phantom should maximally imitate the studied tissues [15]. We proceeded from the fact that the phantom fabrication procedure should be relatively simple and reproducible. We used a polyacrylamide phantom as the most appropriate type of phantom for modeling the effects of laser exposure on brain tumor tissue. The advantages of such a phantom include transparency, high stability (melting point much higher than 100°C), lack of toxicity, and easy modulation of mechanical properties by changing the concentration of acrylamide/methylenebisacrylamide.

In the manufacture of the phantom, we used data from A.H. Negussie [9, 16], according to which 40% acrylamide/bisacrylamide is mixed with water in a ratio of 1:4.4 (241 ml : 1053 ml). In our study, the ratio corresponded to 1:4.7, which is almost identical. For this phantom, the density corresponds to 1033±1.0 kg/m^3, the thermal conductivity coefficient is 0.590±0.015 W/(m·K), and the thermal diffusivity is 0.145±0.002 mm^2/s. These values are close to those for human soft tissues [17]. According to A. Mohammadi [1], the thermal conductivity index for brain tissue corresponds to 0.563 W/(m·K), thermal diffusivity is 0.147 mm^2/sec.

The phantom was made from the following components:

1. Distilled water. When using laser radiation, there is no need for degassing.

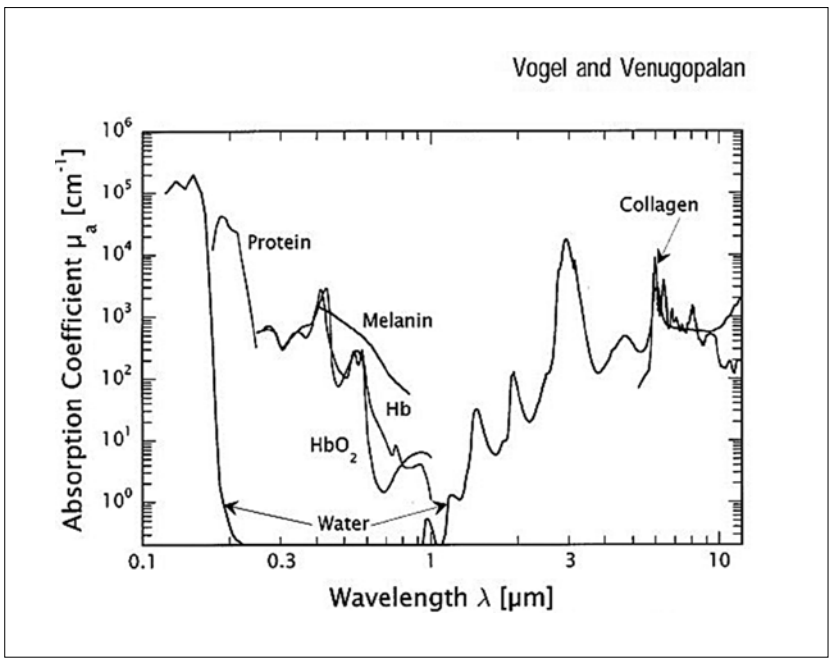

Рис. 1. Коэффициент абсорбции основных тканевых хромофоров для длин волн 100-12000 нм [14] с указанием положения лазерных линий 970 нм и 1560 нм.
Fig. 1. Absorption coefficient of the main tissue chromophores for wavelengths of 100-12000 nm [14] indicating the position of the laser lines 970 nm and 1560 nm.

2. Lyophilised powder of BSA used to detect temperature changes in the phantom and scattering agent. The final concentration of BSA is not less than 5%.

3. Aqueous 40% solution of acrylamide/bisacrylamide, with a weight ratio of acrylamide and bisacrylamide equal to 19:1. The solution is stored at a temperature of 2 to 8°C.

4. Tris/HCl buffer, 1M solution, pH 8.0 (manufacturer – SPD RENAM, Russia).

5. Ammonium persulfate 10% solution for polymerization, prepared ex tempore**.**

6. Hemoglobin (absorbing agent). Citrated blood was used at a ratio of 1 part 3.2% citrate/9 parts whole blood. The formed elements of the blood serve as a scattering agent.

7. TEMED is a polymerizing agent.

8. Sodium azide is a phantom preservative.

To prepare the phantom, we used the following recipe. To 50 ml of distilled degassed water add 5 g of BSA. Stir until complete transition of BSA into solution. Next, 17.5 ml of a 40% acrylamide/bisacrylamide solution, 10 ml of 1M Tris/HCl buffer (pH 8.0) and 600 µl of a 10% ammonium persulfate solution are successively added to the mixture with stirring. Stir until completely homogeneous. Then add citrated blood in an amount depending on the design of the experiment, starting from 750 µl of blood/100 ml phantom. The volume of the mixture is brought to 100 ml with distilled water, then 200 µl of TEMED is added with stirring, the solution is transferred into a round plastic container. Polymerization occurs within 5-10 minutes. In order to prevent dehydration, the resulting gel is stored in a refrigerator in a closed polyethylene container.

To assess the thermal effects, we used a setup that included a two-wave laser apparatus LSP (IRE-Polyus, Fryazino), a miniature thermal imager in the form of an attachment to a smartphone, and a T-8 digital thermograph based on a laptop with thermal sensors. The installation view is schematically shown in Fig. 2.

The phantom was loaded into plastic containers, into which an optical fiber and a thermal sensor were inserted through holes in the side wall (Fig. 3).

The FLIRONE PRO for IOS thermal imager was connected to a smartphone, the display of which displayed a thermal imaging picture with temperature values at selected points, which were recorded in photo and video mode (Fig. 4).

We used a light guide with a direct output of radiation, the modes of which are suitable for use in hyperthermia of brain tumors (Table 1).

Two types of phantom were tested with a lower (F1: 101 mg hemoglobin) and a higher (F2: 202 mg hemoglobin) hemoglobin content. F1 was a model for low- and moderately vascularized tumors, F2 was

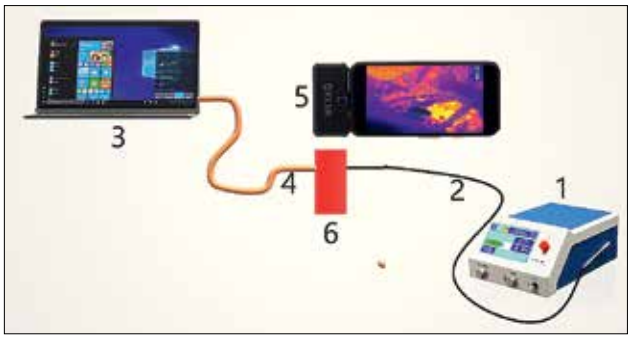

Рис. 2. Установка для изучения влияния лазерного излучения на оптический биофантом: 1 – лазерный аппарат ЛСП («ИРЭ-Полюс», г. Фрязино), 2 – световолокно в держателе, 3 – цифровой термограф Т-8 на базе ноутбука, 4 – термосенсоры, 5 – тепловизионная приставка FLIR ONE PRO for IOS (Китай) вместе со смартфоном iphone 12, 6 – биофантом в контейнере.
Fig. 2. Installation for studying the effect of laser radiation on an optical biophantom. numbers indicate: 1 – laser device LSP ("IRE-Polyus", Fryazino), 2 – optical fiber in the holder, 3 – digital thermograph T-8 based on a laptop with thermal sensors – 4, 5 – thermal imaging attachment FLIR ONE PRO for IOS (China) together with an iphone 12 smartphone, 6 – a biophant in a container.

Рис. 3. Внешний вид контейнера с фантомом: в фантом введено световолокно (1), через торец которого наблюдается пилотное лазерное свечение; рядом с торцом установлен термосенсор (2).
Fig. 3. Appearance of the phantom container: an optical fiber (1) is introduced into the phantom, through the end of which a pilot laser glow is observed; a thermosensor (2) is installed near the end face.

Рис. 4. Внешний вид тепловизора FLIRONE PRO for IOS. Стрелка указывает на тепловизор, расположенный как приставка к смартфону над фантомом.
Fig. 4. Appearance of FLIRONE PRO for IOS thermal imager. The arrow points to a thermal imager located as a prefix to a smartphone above the phantom.

Таблица 1
Характеристики используемого лазерного излучения
Table 1
Characteristics of the laser radiation used

Длина волны (нм) Wavelength (nm)	Мощность излучения (Вт) Radiation power (W)	Время облучения (с) Irradiation time (s)	Энергия (Дж) Energy (J)
970	2	60	120
1560	2	60	120
970+1560	2	60	120

a tumor model with a more developed vascular network. The used modes of laser hyperthermia clearly showed heating zones in the form of clouding of the phantom. The size of the clouded zone varied from 4.5 to 5.5 mm (Fig. 5).

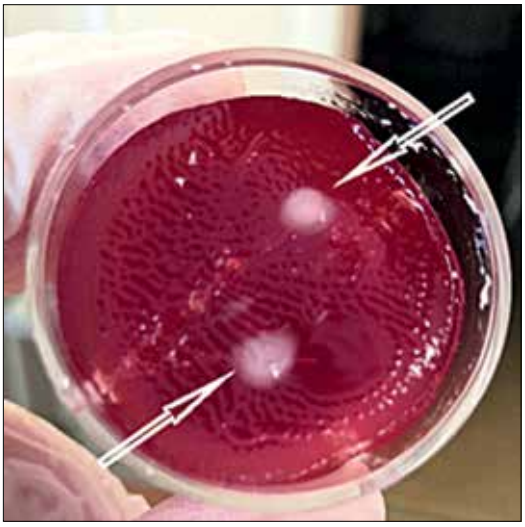

Рис. 5. Фантом. Стрелками показаны зоны помутнения в результате лазерного облучения.
Fig. 5. Phantom. The arrows show the turbidity zones as a result of laser irradiation.

Evaluation of the features of the biophantom coagulation process and the size of the laser coagulation zone at a wavelength of 970 nm and 1560 nm was carried out separately for each of the radiations, or with their combined action. The combined effect of radiation was evaluated under both sequential and simultaneous exposure to the studied wavelengths (Table 2).

Results

The cloudy area of the phantom had an oval-rounded shape. It was noted that in the F2 model, the 970 nm laser radiation creates phantom clouding, propagating anteriorly from the tip of the optical fiber, while the 1560 nm beam was observed to propagate phantom clouding, propagating both forward and posteriorly from the fiber tip. This indicates the difference in both the optical properties of the phantom for different wavelengths and the difference in interaction with chromophores. The combination of two wavelengths in equal proportions demonstrated the dominance of the effects of the 970 nm wavelength, which was also noticed in earlier own studies.

The study of the visual effects of phantom coagulation showed that the maximum area of the coagulation zone when exposed to a wavelength of 1560 nm reached 141.3 mm^2, which is three times more than when exposed to a wavelength of 970 nm (area 47.1 mm^2). The average values of the coagulation spot area were 43.2 (39.3-47.1) mm^2 for 970 nm radiation, and 99.4 (56.5-141.3) mm^2 for 1560 nm radiation (p=0.41). Although the areas of the coagulation spot differed by more than 2 times, the statistical difference was not significant, possibly due to the limited number of experiments. Irradiation with a wavelength of 1560 nm in all cases gave greater heating of the biophantom, which is of great practical importance. Based on the experimental data obtained, further exposure was used with a power of not more than 2 W, with a total energy dose not exceeding 120 J.

The results of laser exposure to the biophantom were visualized in real time using a FLUM-LL fluorescent organoscope [18], which provides multispectral image recording separately in RGB channels in photo and video modes with a resolution of 1280x1024 and a frame rate of 14 Hz (Sony). Although the spectral range of this system is formally limited by a wavelength of 1000 nm, the high brightness of laser radiation made it possible to record a pattern created not only by a 970 nm laser, but also by a 1560 nm laser. The image scale was controlled using a plastic stationery ruler installed directly on the phantom at the time of shooting (Figs. 6 and 7).

From the point of view of the practical use of these wavelengths in the surgery of glial brain tumors,

Таблица 2
Результаты облучения биофантома лазерным излучением с длиной волны 970 нм и 1560 нм
Table 2
Results of irradiation of the biophantom with laser radiation with wavelengths of 970 nm and 1560 nm

Длина волны (нм) Wave length (nm)	Мощность (Вт) Power (W)	Экспозиция (с) Exposure (s)	Энергия (Дж) Energy (J)	Зона коагуляции (мм) Coagulation zone (mm)	Площадь пятна (мм²) Spot area (mm²)	Эффекты коагуляции Effects of coagulation
Облучение одной длиной волны Single wavelength irradiation						
970	2	60	120	5x3	47,1	помутнение фантома clouding of the phantom
1560	2	60	120	9x5	141,3	помутнение фантома clouding of the phantom
Одномоментное облучение двумя длинами волн Simultaneous irradiation with two wavelengths						
970 560	2 2 суммарно total 4	60	240	10x4	125,6	отчетливо слышны щелчки в зоне помутнения фантома clearly audible clicks in the phantom clouding zone
970 1560	1,5 0,5 суммарно total 2	60	120	5x2,5	39,3	помутнение фантома clouding of the phantom
970 1560	0,5 1,5 суммарно total 2	60	120	6x3	56,5	немного слабых щелчков в зоне помутнения фантома a few weak clicks in the phantom clouding zone
970 1560	0,5 2,5 суммарно total 3	60	150	8x4	100,5	немного слабых щелчков в зоне помутнения фантома a few weak clicks in the phantom clouding zone
Последовательное облучение биофантома Sequential biophantome irradiation						
1560 970	2 2	60 60	120 120	7x3	65,9	-
970 1560	2 2	60 60	120 120	7x4 8x5 (повтор)	87,9 125,6	помутнение фантома clouding of the phantom

an important factor was a smoothly and uniformly progressing increase in the area of clouding of the round-oval phantom due to protein coagulation. We did not observe boiling, phantom evaporation, gas bubbles, or smoke. When the phantom was heated, there were no noises, clicks, crackles, etc. This fact indicates the optimal performance of laser radiation for a smooth increase in temperature to 82.8°C from the point of view of safety for the use in brain tumor surgery.

Thermometry

The measurement and distribution of temperature in the phantom as a result of laser irradiation was carried out both using a thermal sensor located near the tip of the optical fiber and using a thermal imaging attachment

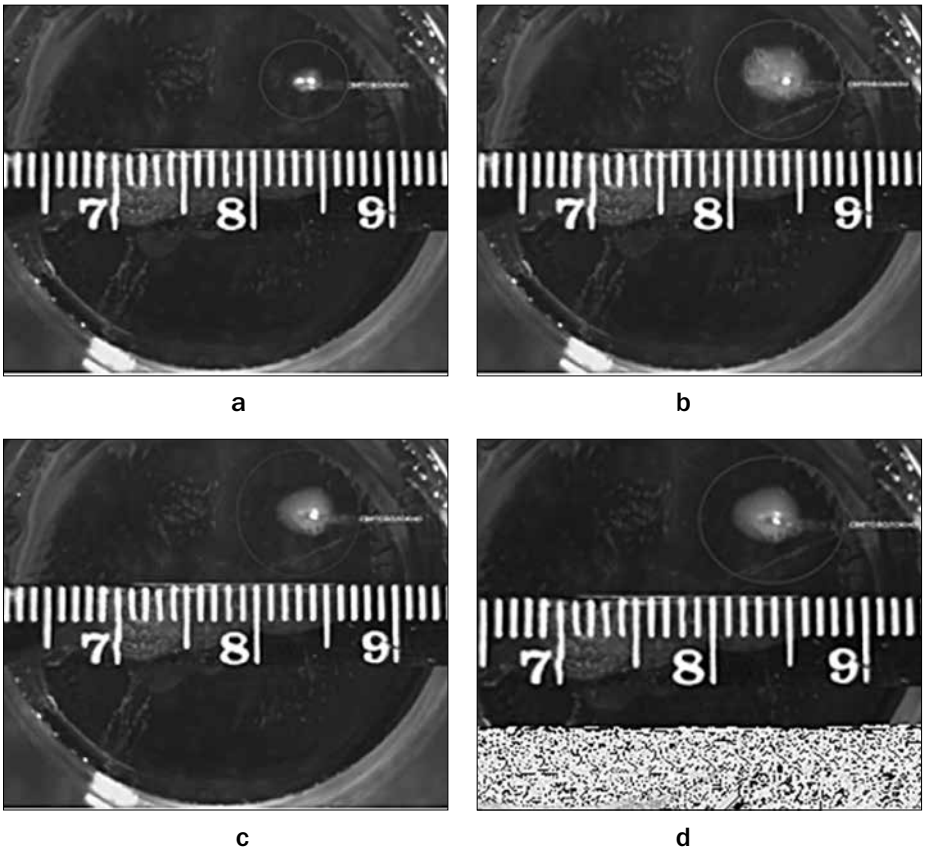

Рис. 6. Визуализация развивающейся зоны коагуляции (выделено кружком) при воздействии на участок фантома лазерным излучением 1560 нм:
a – на 5 с облучения; b – на 20 с;
c – на 40 с; d – на 60 с.
Fig. 6. Visualization of the developing coagulation zone (highlighted by a circle) when the phantom site is exposed to 1560 nm laser radiation:
a – for 5 s of radiation; b – for 20 s;
c – for 40 s; d – for 60 s.

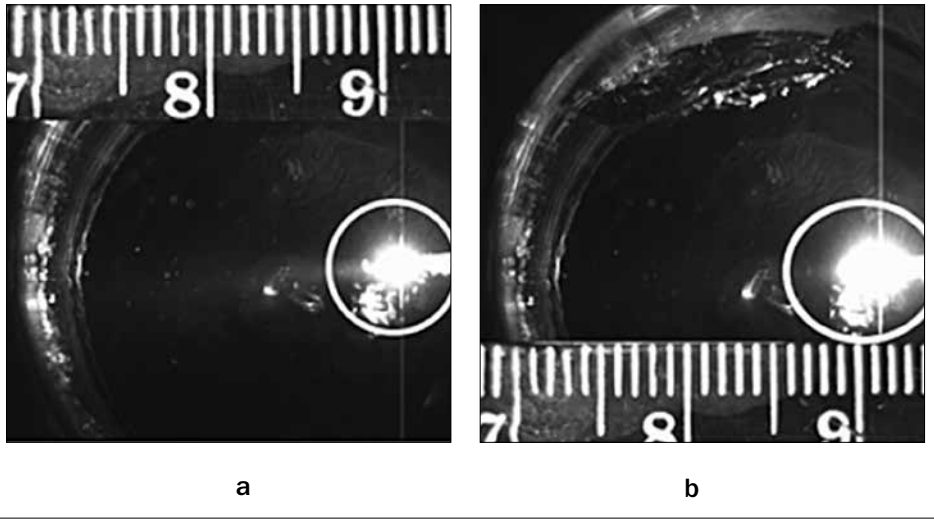

Рис. 7. Распределение лазерного излучения 970 нм в фантоме: a – 5 с воздействия; b – 60 с воздействия.
Fig. 7. Distribution of 970 nm laser radiation in the phantom: a – 5th s of exposure; b – 60th s of exposure.

for a FLIRONE PRO for IOS smartphone, fixed above the phantom (see Fig. 4). The thermal imaging attachment made it possible to estimate the temperature distribution in various parts of the phantom by registering the radiation pattern of the object in the infrared region. Thus, it was possible to simultaneously record the temperature in real time both with the help of a thermal sensor fixed at a distance of 3 mm from the end of the light guide and at three points of the thermal image selected at a distance of about 2 mm from one another. An example of a thermal image of the temperature distribution and the results of its evaluation at 3 points near the end of the optical fiber at the end of 60 s of laser irradiation is shown in Fig. 8. The temperature equal to 82.8°C in the center of irradiation indicated coagulation in this zone. Such a temperature gradient from the fiber tip correlates with *ex vivo* thermometry literature data [19].

Dynamic measurements of the temperature of the F1 phantom at the tip of the optical fiber using a digital thermograph, performed in a constant irradiation mode at a wavelength of 1560 nm, established a relatively rapid increase in temperature in the first 10 s. After 20 s, the temperature changed slightly, averaging 71.8°C (Fig. 9).

When the F1 phantom (with a lower hemoglobin concentration) was irradiated with a laser with a wavelength of 970 nm, a less dynamic and lower heating temperature of the phantom was obtained. In 60 s, it gradually increased from room temperature to 50°C (Fig. 10).

When the phantom was irradiated with a combination of 1560 nm and 970 nm wavelengths with a total power of 2 W, a gradual rise in temperature was also observed, resembling the course of the curve for the 970 nm wave, but reaching a higher level (88°C) with some decrease after 50 s of irradiation. The average temperature during irradiation was 66.9°C (Fig. 11).

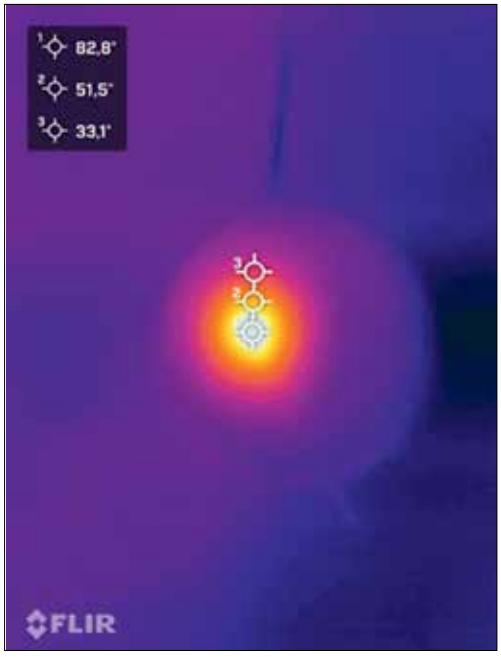

Рис. 8. Тепловизионное изображение участка фантома. Параметры температуры в 3 точках фантома на 60 с облучения длиной волны 1560 нм: 82,8°С у кончика световолокна; 51,5°С на расстоянии 2 мм и 33,1°С на расстоянии 4 мм от кончика световолокна.
Fig. 8. Thermal imaging of the phantom site. Temperature parameters in 3 points of the phantom on the 60th with exposure to a wavelength of 1560 nm: 82.8°C at the tip of the fiber; 51.5°C at a distance of 2 mm and 33.1°C at a distance of 4 mm from the tip of the fiber.

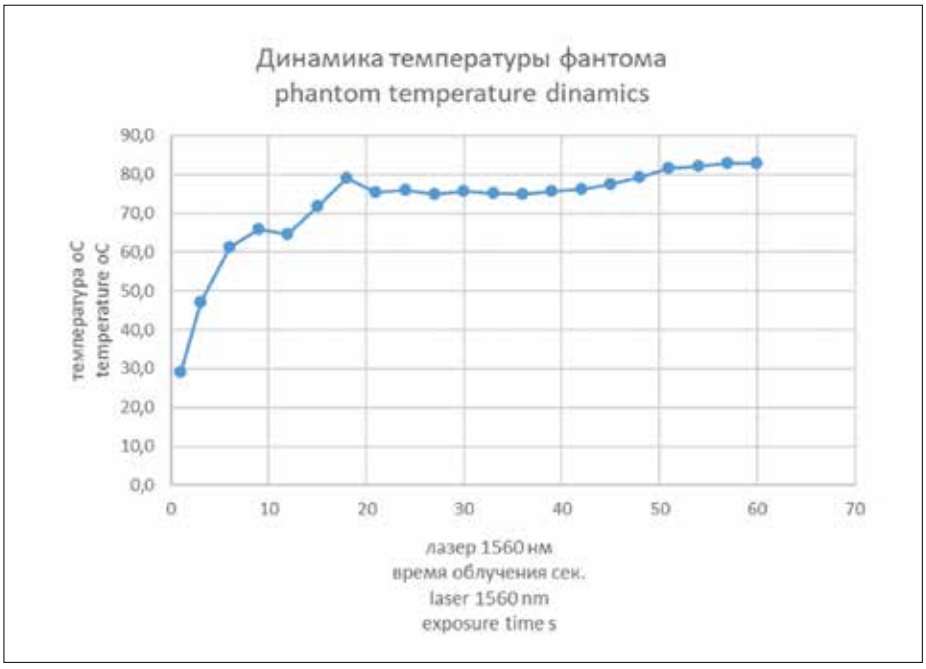

Рис. 9. Динамика температуры фантома при лазерном облучении на длине волны 1560 нм, мощность 2 Вт.
Fig. 9. The temperature dynamics of the phantom under irradiation with a 1560 nm laser, 2 W power.

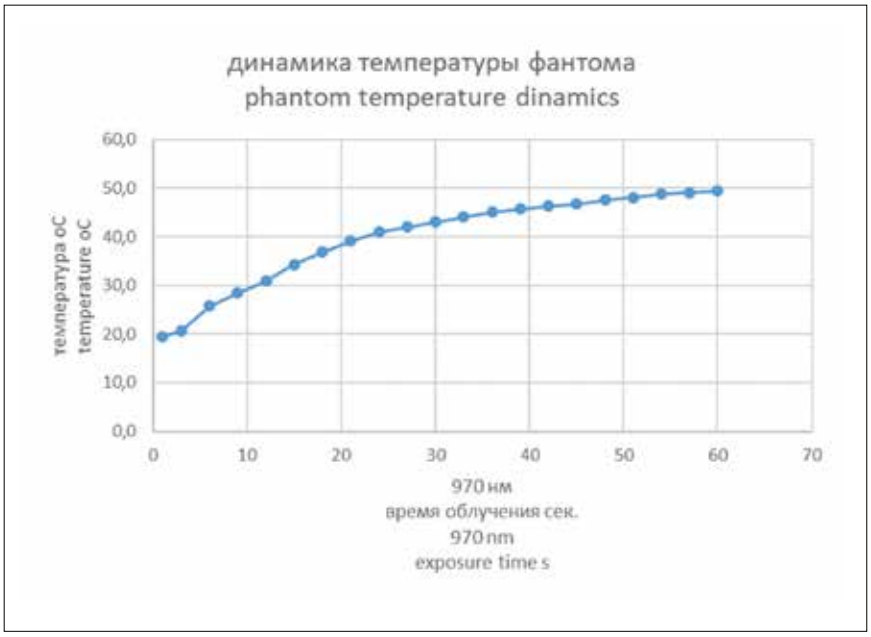

Рис. 10. Динамика температуры фантома при лазерном облучении на длине волны 970 нм, мощность 2 Вт.
Fig. 10. The temperature dynamics of the phantom under irradiation with a 970 nm laser, 2 W power.

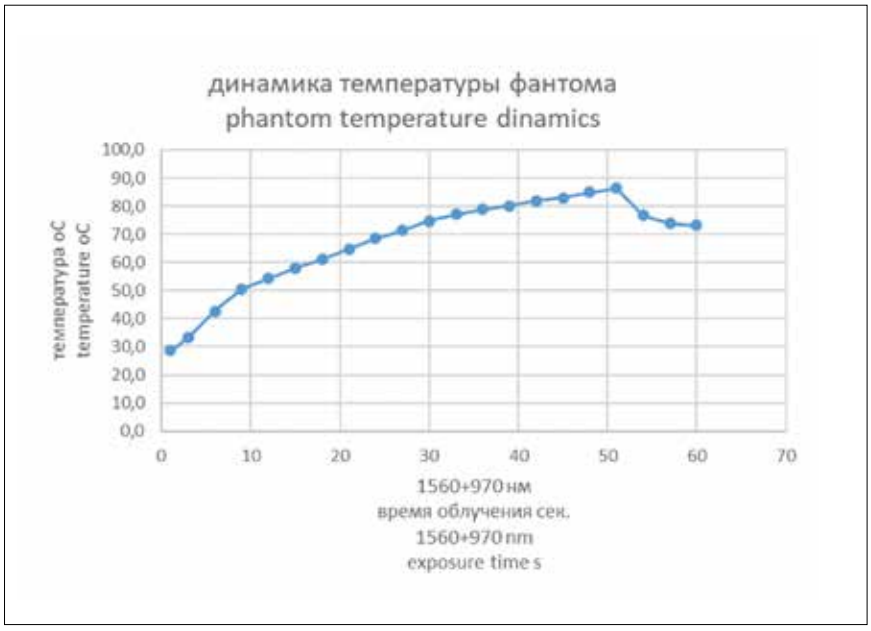

Рис. 11. Динамика температуры фантома у кончика световолокна, при синхронном облучении лазером волнами длиной 1560 нм и 970 нм.
Fig. 11. The temperature dynamics of the phantom at the tip of the optical fiber, during synchronous irradiation with a laser of 1560 nm and 970 nm.

The uneven heating of the phantom observed during irradiation at a wavelength of 1560 nm or a combination of radiation with a wavelength of 970 nm and 1560 nm can be explained by a phase transition of the second type of substance due to heating [20].

Discussion

Thus, the real-time video recording of the process of laser irradiation by the camera visually demonstrated the process of phantom hyperthermia as a brain tumor model. The smoothness of heating, the safe achievement of the coagulation temperatures of the modes used and the dose of laser radiation have been confirmed. The absence of phantom boiling, gas and smoke formation indicates that the temperature in the zone of interaction between the phantom and the laser beam is less than 100°C, which is supported in the methodology of hyperthermia of brain tumors. This fact

was also confirmed by us in an experiment with direct temperature measurement by thermosensors and a thermal imager. This study showed differences in the use of radiation at two wavelengths in temperature effects, sizes of coagulation zones, features of the distribution of the coagulation zone in relation to the tip of the optical fiber. We observed all these effects with the F1 phantom containing a lower concentration of hemoglobin and used as a model of a weakly or moderately vascularized tumor. The F2 phantom with a high hemoglobin content showed coagulation only immediately near the tip of the optical fiber. These features of the interaction should be taken into account when planning the operation, well visualizing areas of the tumor with hypervascularization.

Both methods of temperature measurement demonstrated its smooth rise during irradiation. The farther from the tip of the optical fiber was the thermocouple probe or the temperature measurement point of the thermal imager, the lower the temperature. The difference between temperature measurements by a thermocouple and a thermal imager reached 7°C. This insignificant measurement error by two different methods can be explained by the fact that the thermocouple measures the temperature inside the phantom, while the thermal imager measures the temperature from its surface [21]. Therefore, when fixing the temperature with a thermal imager, we placed the optical fiber at a depth of 1 mm from the phantom surface.

The work was performed on two types of phantoms differing in hemoglobin concentration. This choice was made due to the fact that we consider it important to separate the effects of laser exposure on tumors with different degrees of vascularization, which is due to differences in the level of hemoglobin in tumors. Differences in blood supply require a differentiated approach to the practical application of the laser hyperthermia methodology. Methods for fixing the temperature in a phantom during laser irradiation have been developed and tested. Based on the temperature indicators, it was found that when using real operating modes, the temperature does not exceed 83°C, does not reach the boiling point, the evaporation of the phantom. This confirms the delicacy and safety of these regimens in achieving tumor coagulation. Despite the fact that, in contrast to a tumor, there is no microcirculation in the phantom, this work made it possible to reveal differences in the interaction with the phantom of the two wavelengths used. The obtained results confirm the correctness of the chosen modes of interstitial laser irradiation in minimally invasive hyperthermia of intracerebral tumors.

Conclusion

The heating zone at 1560 nm is always larger than at 970 nm irradiation. Using an irradiation power of more than 2 W, on the one hand, increases the coagulation zone, but audible clicks appear, which indicates ablation of the phantom, boiling due to an increase in temperature above 100°C. Therefore, exceeding the power of interstitial laser radiation by more than 2 W is inappropriate, since it may be associated with undesirable effects in the tumor tissue and the surrounding brain tissue and its vessels. With total irradiation with two waves, the coagulation zone is the larger, the greater the radiation power of 1560 nm. The result of coagulation during sequential irradiation of the biophantom depends little on the sequence of the chosen wavelength. It should be taken into account that when irradiated with a wave of 970 nm, the coagulation zone partially propagates posterior to the tip of the optical fiber; at a length of 1560 nm, almost the entire coagulation zone occurs anterior to the fiber tip. This indicates differences in the interaction and in the optical properties of these two wavelengths with respect to the phantom. The 970 nm radiation propagates less forward, showing smaller penetration in the phantom. The spread of coagulation posteriorly from the tip of the optical fiber is a consequence of the predominance of the reflection of light or the movement of thermal energy posteriorly. All these differences in the distribution of the coagulation zone and temperature dynamics are important to take into account both when planning treatment and in the practical application of the technology of minimally invasive hyperthermia of intracerebral tumors.

REFERENCES

1. Mohammadi A., Bianchi L., Asadi S., Saccomandi P. Measurement of Ex Vivo Liver, Brain and Pancreas Thermal Properties as Function of Temperature. *Sensors (Basel)*, 2021, vol. 21(12), pp. 4236. doi: 10.3390/s21124236
2. Ahmed M., Brace C.L., Fred T Lee Jr. F.T., Goldberg S.N. Principles of and advances in percutaneous ablation. *Radiology*, 2011, vol. 258(2), pp. 351-69. doi: 10.1148/radiol.10081634
3. Franzini A., Moosa S., Servello D., Small I., DiMeco F., Xu Z., Elias W.J., Franzini A., Prada F. Ablative brain surgery: an overview. *Int. J. Hyperth.*, 2019, vol. 36, pp. 64–80. doi: 10.1080/02656736.2019.1616833
4. Geoghegan R., Ter Haar G., Nightingale K., Marks L., Natarajan S. Methods of monitoring thermal ablation of soft tissue tumors - A

ЛИТЕРАТУРА

1. Mohammadi A., Bianchi L., Asadi S., Saccomandi P. Measurement of Ex Vivo Liver, Brain and Pancreas Thermal Properties as Function of Temperature // Sensors (Basel). – 2021. – Vol. 21(12). – P. 4236. doi: 10.3390/s21124236
2. Ahmed M., Brace C.L., Fred T Lee Jr. F.T., Goldberg S.N. Principles of and advances in percutaneous ablation // Radiology. – 2011. – Vol. 258(2). – P. 351-69. doi: 10.1148/radiol.10081634
3. Franzini A., Moosa S., Servello D., Small I., DiMeco F., Xu Z., Elias W.J., Franzini A., Prada F. Ablative brain surgery: an overview // Int. J. Hyperth. – 2019. – Vol. 36. – P. 64–80. doi:10.1080/02656736.2019.1616833
4. Geoghegan R., Ter Haar G., Nightingale K., Marks L., Natarajan S. Methods of monitoring thermal ablation of soft tissue tumors - A

comprehensive review. *Med. Phys.*, 2022, vol. 49(2), pp.769-791. doi: 10.1002/mp.15439

5. Chen C., Lee I., Tatsui C., Elder T., Sloan A.E. Laser interstitial thermotherapy (LITT) for the treatment of tumors of the brain and spine: a brief review. *J. of Neuro-Oncology*, 2021, vol. 151, pp. 429–442. doi: 10.1007/s11060-020-03652-z
6. Lagman C., Chung L.K., Pelargos P.E., Ung N., Bui T.T., Lee S.J., Voth B.L., Yang I. Laser neurosurgery: A systematic analysis of magnetic resonance-guided laser interstitial thermal therapies. *J. Clin. Neurosci.*, 2017, vol. 36, pp. 20-26. doi: 10.1016/j.jocn.2016.10.019
7. Ostreyko O.V., Mozhaev S.V. Way of treatment of glial tumors of a brain of supratentorialny localization. Patent of the Russian Federation for invention No. 2533032 of 16.09.2014.
8. Eranki A., Mikhaila A.S., Negussiea A.H., Prateek S.K., Wooda B.J., Partanen A. Tissue-mimicking thermochromic phantom for characterization of HIFU devices and applications, *International Journal of Hyperthermia*, 2019, vol. 36(1), pp. 518-529. doi: 10.1080/02656736.2019.1605458
9. Negussie A.H., Partanen A., Mikhail A.S., Xu S., Abi-Jaoudeh N., Maruvada S., Wood B.J. Thermochromic tissue-mimicking phantom for optimisation of thermal tumour ablation. *Int. J. Hyperthermia*, 2016, vol. 32(3), pp. 239-43. doi: 10.3109/02656736.2016.1145745
10. Dabbagh A., Jeet Abdullah B.J., Abu Kasim N.H., Ramasindarum C. Reusable heat-sensitive phantom for precise estimation of thermal profile in hyperthermia application. *Int. J. Hyperthermia*, 2014, vol. 30(1), pp. 66-74. doi: 10.3109/02656736.2013.854930
11. Bazrafshan B., Hubner F., Farshid P., Larson M.C., Vogel V., Mantele W., Vogl T.J. A liver-mimicking MRI phantom for thermal ablation experiments. *Med. Phys.*, 2011, vol. 38, pp. 2674–84. doi: 10.1118/1.3570577
12. Davidson S.R.H., Sherar M.D. Measurement of the thermal conductivity of polyacrylamide tissue-equivalent material. *Int. J. Hyperthermia*, 2003, vol. 19(5), pp. 551-62. doi: 10.1080/0265673031000160799 5
13. Ningrum E.O., Purwanto A., Rosita G.C., Bagus A. The Properties of Thermosensitive Zwitterionic Sulfobetaine NIPAM-co-DMAAPS Polymer and the Hydrogels: The Effects of Monomer Concentration on the Transition Temperature and Its Correlation with the Adsorption Behavior. *Indones. J. Chem.*, 2020, vol. 20 (2), pp. 324-335. doi: 10.22146/ijc.41499
14. Vogel A., Venugopoplan V. Mechanisms of Pulsed Laser Ablation of Biological Tissues. *Chem. Rev.*, 2003, vol. 103, pp. 577–644. doi:10.1021/cr030683b
15. Minton J.A., Iravani A., Yousefi A. Improving the homogeneity of tissue-mimicking cryogel phantoms for medical imaging, *Med. Phys.*, 2012, vol. 39(11), pp. 6796-807. doi: 10.1118/1.4757617
16. Guntur S.R., Choi M.J. An improved tissue-mimicking polyacrylamide hydrogel phantom for visualizing thermal lesions with high-intensity focused ultrasound. *Ultrasound in med. and biol.*, 2014, vol. 40(11), pp. 2680-2691. doi: 10.1016/j.ultrasmedbio.2014.06.010
17. Welch A.J., Gemert M.J.C. Optical-thermal response of laser-irradiation tissue. *Springer*, 2011, 947 p. https://doi:10.1007/978-90-481-8831-4
18. Kang U.K., Papayan G.V., Berezin I.B., Jin Bae-Soo, Kim S.V., Petrishchev N.N. Multispectral fluorescent organoscopes for in vivo studies of laboratory animals and their organs. *Optical Journal*, 2011, vol. 78(9), pp. 82-90. (in Russ.). OCIS codes: 170.0170, 170.3880, 170.3890, 170.4580
19. Korganbayev S., Orrico A., Bianchi L., De Landro M., Wolf A., Dostovalov A., Saccomandi P. Closed-Loop Temperature Control Based on Fiber Bragg Grating Sensors for Laser Ablation of Hepatic Tissue. *Sensors 2020*, vol. 20(22), 6496. doi: 10.3390/s20226496
20. Manns F., Milne P.J, Gonzalez-Cirre X., Denham, D.B, Parel J., Robinson D.S. In situ temperature measurements with thermocouple probes during laser Interstitial thermotherapy (LITT): quantification and correction of a measurement artifact. *Lasers Surg. Med.*, 1998, vol. 23(2), pp. 94–103. doi: 10.1002/(sici)1096-9101(1998)23:2<94::aid-lsm7>3.0.co;2-q

comprehensive review // Med. Phys. – 2022. – Vol. 49(2). – P. 769-791. doi: 10.1002/mp.15439

5. Chen C., Lee I., Tatsui C., Elder T., Sloan A.E. Laser interstitial thermotherapy (LITT) for the treatment of tumors of the brain and spine: a brief review // J. of Neuro-Oncology. – 2021. – Vol. 151. – P. 429–442. doi: 10.1007/s11060-020-03652-z
6. Lagman C., Chung L.K., Pelargos P.E., Ung N., Bui T.T., Lee S.J., Voth B.L., Yang I. Laser neurosurgery: A systematic analysis of magnetic resonance-guided laser interstitial thermal therapies // J. Clin. Neurosci. – 2017. – Vol. 36. – P. 20-26. doi: 10.1016/j.jocn.2016.10.019
7. Острейко О.В., Можаев С.В. Способ лечения глиальных опухолей головного мозга супратенториальной локализации // Патент РФ на изобретение №2533032 от 16.09.2014.
8. Eranki A., Mikhaila A.S., Negussiea A.H., Prateek S.K., Wooda B.J., Partanen A. Tissue-mimicking thermochromic phantom for characterization of HIFU devices and applications // International Journal of Hyperthermia. – 2019. – Vol. 36(1). – P. 518-529. doi: 10.1080/02656736.2019.1605458
9. Negussie A.H., Partanen A., Mikhail A.S., Xu S., Abi-Jaoudeh N., Maruvada S., Wood B.J. Thermochromic tissue-mimicking phantom for optimisation of thermal tumour ablation // Int. J. Hyperthermia. – 2016. – Vol. 32(3). – P. 239-43. doi: 10.3109/02656736.2016.1145745
10. Dabbagh A., Jeet Abdullah B.J., Abu Kasim N.H., Ramasindarum C. Reusable heat-sensitive phantom for precise estimation of thermal profile in hyperthermia application // Int. J. Hyperthermia. – 2014. – Vol. 30(1). – P. 66-74. doi: 10.3109/02656736.2013.854930
11. Bazrafshan B., Hubner F., Farshid P., Larson M.C., Vogel V., Mantele W., Vogl T.J. A liver-mimicking MRI phantom for thermal ablation experiments // Med. Phys. – 2011. – Vol. 38. – P. 2674–84. doi: 10.1118/1.3570577
12. Davidson S.R.H., Sherar M.D. Measurement of the thermal conductivity of polyacrylamide tissue-equivalent material // Int. J. Hyperthermia. – 2003. – Vol. 19(5). – P. 551-62. doi: 10.1080/0265673031000160799 5
13. Ningrum E.O., Purwanto A., Rosita G.C., Bagus A. The Properties of Thermosensitive Zwitterionic Sulfobetaine NIPAM-co-DMAAPS Polymer and the Hydrogels: The Effects of Monomer Concentration on the Transition Temperature and Its Correlation with the Adsorption Behavior // Indones. J. Chem. – 2020. – Vol. 20 (2). – P. 324-335. doi: 10.22146/ijc.41499
14. Vogel A., Venugopoplan V. Mechanisms of Pulsed Laser Ablation of Biological Tissues // Chem. Rev. – 2003. – Vol. 103. – P. 577–644. doi: 10.1021/cr030683b
15. Minton J.A., Iravani A., Yousefi A. Improving the homogeneity of tissue-mimicking cryogel phantoms for medical imaging // Med. Phys. – 2012. – Vol. 39(11). – P. 6796-807. doi: 10.1118/1.4757617
16. Guntur S.R., Choi M.J. An improved tissue-mimicking polyacrylamide hydrogel phantom for visualizing thermal lesions with high-intensity focused ultrasound // Ultrasound in med. and biol. – 2014. – Vol. 40(11). – P. 2680-2691. doi: 10.1016/j.ultrasmedbio.2014.06.010
17. Welch A.J., Gemert M.J.C. Optical-thermal response of laser-irradiation tissue. // Springer. – 2011. – 947 p. doi:10.1007/978-90-481-8831-4
18. Kang U.K., Папаян Г.В., Березин И.Б., Jin Bae-Soo, Ким С.В., Петрищев Н.Н. Мультиспектральные флуоресцентные органоскопы для прижизненных исследований лабораторных животных и их органов // Оптический журнал. –2011. – Vol. 78(9). – P. 82-90.
19. Korganbayev S., Orrico A., Bianchi L., De Landro M., Wolf A., Dostovalov A., Saccomandi P. Closed-Loop Temperature Control Based on Fiber Bragg Grating Sensors for Laser Ablation of Hepatic Tissue // Sensors 2020. – Vol. 20(22). – P. 6496. doi.org/10.3390/s20226496
20. Manns F., Milne P.J, Gonzalez-Cirre X., Denham, D.B, Parel J., Robinson D.S. In situ temperature measurements with thermocouple probes during laser Interstitial thermotherapy (LITT): quantification and correction of a measurement artifact // Lasers Surg. Med. – 1998. – Vol. 23(2). – P. 94–103. doi: 10.1002/(sici)1096-9101(1998)23:2<94::aid-lsm7>3.0.co;2-q

STUDY OF ACUTE TOXICITY OF MONOCATIONIC CHLORIN e6 DERIVATIVE, A PERSPECTIVE PHOTOSENSITIZER FOR ANTIMICROBIAL AND ANTITUMOR PHOTODYNAMIC THERAPY

Zhidomorov N.Yu.[1], Nazarenko O.A.[1], Demidov V.I.[1], Kustov A.V.[2,3], Kukushkina N.V.[2,3], Koifman O.I.[2,3], Gagua A.K.[4], Tomilova I.K.[1], Berezin D.B.[3]
[1]Ivanovo State Medical Academy, Ivanovo, Russia
[2]G.A. Krestov Institute of Solution Chemistry of the Russian Academy of Sciences, Ivanovo, Russia
[3]Ivanovo State University of Chemistry and Technology, Research Institute of Macroheterocycles, Ivanovo, Russia
[4]National Medical Research Center for Otorhinolaryngology of the Federal Medico-Biological Agency of Russia, Moscow, Russia

Abstract

In this experimental work the acute toxicity of a chemically modified derivative of the natural pigment chlorophyll *a* called monocationic chlorin e6, which is a promising photosensitizer (PS) for antimicrobial and antitumor photodynamic therapy, was studied using white rats. The advantages of the PS under investigation are an intense absorption in the long-wavelength region of the visible spectrum, a sufficiently high quantum yield of singlet oxygen generation, pronounced amphiphilic properties along with an appropriate solubility in water, and a high level of photocytotoxicity in relation to both malignant *HeLa* cells and antibiotic-resistant hospital strains of *E. coli* bacteria., *P. aerugenosa* and others. It has been shown that the value of LD_{50} of the considered PS can be calculated as the value of 100 mg/kg. In the reproduced experimental model of acute toxicity, pathomorphological changes in the vital organs of laboratory animals indicate a pronounced vasopathic effect of the drug with the development of cerebral edema and respiratory distress syndrome, which have become the main signs of thanatogenesis.

Key words: antimicrobial photodynamic therapy, antitumor photodynamic therapy, photosensitizer, chlorins, acute toxicity.

For citations: Zhidomorov N.Yu., Nazarenko O.A., Demidov V.I., Kustov A.V., Kukushkina N.V., Koifman O.I., Gagua A.K., Tomilova I.K., Berezin D.B. Study of acute toxicity of monocationic chlorin e6 derivative, a perspective photosensitizer for antimicrobial and antitumor photodynamic therapy, *Biomedical Photonics*, 2022, vol. 11, no. 2, pp. 23–32. doi: 10.24931/2413–9432–2022–11-2-23-32.

Contacts: Berezin D.B., e-mail: berezin@isuct.ru

ИССЛЕДОВАНИЕ ОСТРОЙ ТОКСИЧНОСТИ МОНОКАТИОННОГО ПРОИЗВОДНОГО ХЛОРИНА e6 – ПЕРСПЕКТИВНОГО ФОТОСЕНСИБИЛИЗАТОРА ДЛЯ АНТИМИКРОБНОЙ И ПРОТИВООПУХОЛЕВОЙ ФОТОДИНАМИЧЕСКОЙ ТЕРАПИИ

Н.Ю. Жидоморов[1], О.А. Назаренко[1], В.И. Демидов[1], А.В. Кустов[2,3], Н.В. Кукушкина[2,3], О.И. Койфман[2,3], А.К. Гагуа[4], И.К. Томилова[1], Д.Б. Березин[3]
[1]Ивановская государственная медицинская академия» Министерства здравоохранения РФ, Иваново, Россия
[2]Институт химии растворов им. Г.А. Крестова Российской академии наук, Иваново, Россия
[3]«Ивановский государственный химико-технологический университет», НИИ Макрогетероциклов, Иваново, Россия
[4]«Национальный медицинский исследовательский центр оториноларингологии» ФМБА, Москва, Россия

ORIGINAL ARTICLES

Резюме

На белых крысах изучены особенности острой токсичности химически модифицированного производного природного пигмента хлорофилла *a* монокатионного хлорина е6 – перспективного фотосенсибилизатора (ФС) для антимикробной и противоопухолевой фотодинамической терапии. Преимуществами ФС являются интенсивное поглощение в длинноволновой области видимого спектра, достаточно высокий квантовый выход генерации синглетного кислорода, выраженные амфифильные свойства наряду с хорошей растворимостью в воде и высокий уровень фотоцитотоксичности в отношении как злокачественных клеток линии *HeLa*, так и антибиотикорезистентных госпитальных штаммов бактерий *E. coli*, *P. Aerugenosa* и других. Величина $ЛД_{50}$ для монокатионного хлорина е6 составляет 100 мг/кг массы тела. В воспроизведенной экспериментальной модели острой токсичности патоморфологические изменения жизненно важных органов лабораторных животных свидетельствуют о выраженном вазопатическом действии препарата с развитием отека головного мозга и респираторного дистресс-синдрома, ставшими основными звеньями танатогенеза.

Ключевые слова: антимикробная фотодинамическая терапия, противоопухолевая фотодинамическая терапия, фотосенсибилизатор, хлорины, острая токсичность.

Для цитирования: Жидоморов Н.Ю., Назаренко О.А., Демидов В.И., Кустов А.В., Кукушкина Н.В., Койфман О.И., Гагуа А.К., Томилова И.К., Березин Д.Б. Исследование острой токсичности монокатионного производного хлорина е6 – перспективного фотосенсибилизатора для антимикробной и противоопухолевой фотодинамической терапии // Biomedical Photonics. – 2022. – Т. 11, № 2. – С. 23–32. doi: 10.24931/2413–9432–2022–11-2-23-32.

Контакты: Березин Д.Б., e-mail: berezin@isuct.ru

Introduction

Photodynamic therapy (PDT) is a sophisticated minimally invasive approach to the treatment of a wide range of oncological diseases and localized microbial infections, which can be used both independently and in combination with surgery, drug and radiation therapy [1–14]. Important advantages of PDT, in addition to its low invasiveness, are the lack of treatment resistance of tumor and microbial cells, as well as the ability of PDT to induce an immune response in the body [2, 4, 5, 9, 11].

The method is based on the selective accumulation in malignant and microbial cells of low-toxic pigments - photosensitizers (PS), capable of interacting with molecular oxygen $^3O_2$ under the action of visible light, triggering a cascade of photochemical reactions. This leads to efficient generation of reactive oxygen species (ROS) and destruction of pathogenic microorganisms or tumor cells [1–3, 10–15]. Depending on the nature of the PS, ROS generation can proceed according to one of two mechanisms: with the formation of singlet oxygen $^1O_2$ or oxygen-bearing radical species, in particular, OH and O_2 [1, 11, 15]. The luminescent red glow of malignant tissue under the action of visible radiation as a result of the selective accumulation of PS in it is used for fluorescence diagnostics (FD) of tumors [7, 12].

To date, a number of PS are used in clinical practice for the diagnosis and treatment of patients with oncological diseases and bacterial infections [1, 6, 8, 11, 16]. Most of the PSs are macroheterocyclic compounds of the class of porphyrins, phthalocyanines, chlorins, or bacteriochlorins [16–20], as well as a number of 5-aminolevulinic acid derivatives. It is important to note that almost all previously developed PDT preparations aimed at combating oncological diseases contain nonionic or anionic substituents in their molecules [11, 21].

Recent studies are aimed primarily at the development and testing of new, more effective third-generation PSs [12, 22]. In addition to intensive absorption of visible radiation in the area of the "therapeutic window" of biological tissues (600–850 nm) and efficient generation of ROS, the main modern requirements for PS are a good hydrophilic-lipophilic balance, which implies simultaneous water and fat solubility (amphiphilicity) of PS, low cost, stability of dosage forms during storage, and, most importantly, low dark and pronounced photocytotoxicity of drugs.

Antimicrobial PDT imposes a number of specific requirements on PS, the main of which is the presence of one or several cationic groups in the structure of the molecule, the positive charge of which significantly increases the affinity of drugs for the cell wall of microorganisms, primarily gram-negative pathogenic bacteria [9–12, 23], since the drugs used for antitumor PDT turned out to be ineffective in photoinactivation of gram-negative microorganisms [11].

Previously, we carried out a series of systematic multidisciplinary studies on the preparation and study of superficially active substances (SAS) soluble in water or aqueous solutions of PS of the porphyrin and chlorin series. The works included the synthesis of PS, evaluation of their generation of singlet oxygen [24–26], determination of solubility, hydrophilic–lipophilic balance, and study of the interaction of PS with potential carriers based on biocompatible polymers and micellar SAS [27–32]. The dark and photoinduced toxicity of drugs against tumor cells and conditionally pathogenic strains of microorganisms was also studied *in vitro* and *in vivo* [14, 25, 26, 33, 34]. Studies have shown that PS with cationic

groups have a pronounced photocytotoxicity against gram-negative bacterial microflora [27, 28, 33, 34] both *in vitro* and *in vivo*. It was found that monocationic derivatives of chlorin e6 can effectively inactivate tumor cell cultures *in vitro* [12, 35], while tricationic chlorins have a weak cytotoxic effect.

Several studied compounds, in particular, the monocationic derivative of chlorin e6 (compound I), have the best combination of characteristics in terms of the above requirements. This PS is fairly well soluble in bidistilled water (more than 1 mmol/kg at 25^{0}C), and in aqueous solutions of potential delivery vehicles - Tween 80 or polyvinylpyrrolidone (PVP), its solubility increases several times. It has intense absorption in the red region of the spectrum (660 nm) and in non-aqueous media effectively generates singlet oxygen with a quantum yield of ~0.6 [27], has a good hydrophilic-lipophilic balance with a distribution coefficient in the system "1-octanol/phosphate-buffer saline", equal to 8.6 ± 0.2 at a temperature of 298 K [27, 29], binds quite strongly to micelles of the nonionic SAS Tween 80 (K_b = 4.57 ± 0.22 in the PS concentration range ~0.01 mmol/kg), being localized mainly near the surface of micelles [30, 31], and also has a pronounced photoinduced antitumor effect (against *HeLa* cells *in vitro*) [35] and antimicrobial activity against both Gram-positive (*St. aureus*) and Gram-negative (*E. coli*) pathogenic flora *in vitro* [27, 33].

The survival index (%) of *HeLa* cancer cells *in vitro* at a PS content of 1 μmol/l after irradiation with red light (660 nm, dose 12 J/cm^2) was only 3.71±0.11 [33], which indicates a pronounced photoinduced antitumor activity of the drug. The authors showed the photocytotoxicity of compound I against archival strains of microorganisms [25, 31], and at a concentration of microbial cells of 10^3 CFU and irradiation with red light (660 nm, S_{PS} = 50 μmol/l) at a dose of 40 J/cm^2, complete inactivation of gram-positive microflora (*St. aureus*) was achieved, while the number of gram-negative bacteria (*E. coli*) did not decrease. The use of additives that contribute to the destabilization of the outer membrane of microorganisms (Tween 80, Trilon B) and/or an increase in PS concentration led to complete photoinactivation of microbes during the experiment [25].

The results of the conducted studies show that compound I has a good potential for use as a PS for PDT. This dictates the need to study the effects associated with the toxic effects of the drug on the living organism as a whole, its organs and systems. Previous studies indicate the extremely low toxicity of anionic PS for PDT based on chlorin e6 [8, 21, 22, 31]. In particular, one of the most commonly used PS of the chlorine series, photolon, has a lethal LD_{50} dose of about 180 mg/kg of body weight, which is 100 times higher than the commonly used doses during PDT [21]. However, the presence of a cationic group in compound I can significantly increase PS cytotoxicity. Thus, information about the features of its effects on the body is essential for further preclinical trials of the drug. The aim of this work is to study the acute toxicity of PS, estimate the LD_{50} value, and study the mechanisms of thanatogenesis of monocationic chlorin e6.

Materials and methods

Synthesis of chlorin (compound I) was carried out from methylpheophorbide *a* (compound II) according to the described two-stage procedure [25, 33, 34]. Methylpheophorbide *a* was obtained by demetallation and partial acid hydrolysis of chlorophyll *a* (compound III) extracted from the cyanobacterium *Spirulina Platensis* [35]. The purity of the obtained final product weighing more than 500 mg, spectrally identified by nuclear magnetic resonance (^{1}H NMR, Bruker 500 Avance III) and mass spectrometry (MALDI, MALDI-TOF Shimadzu Axima Confidence) was at least 95%.

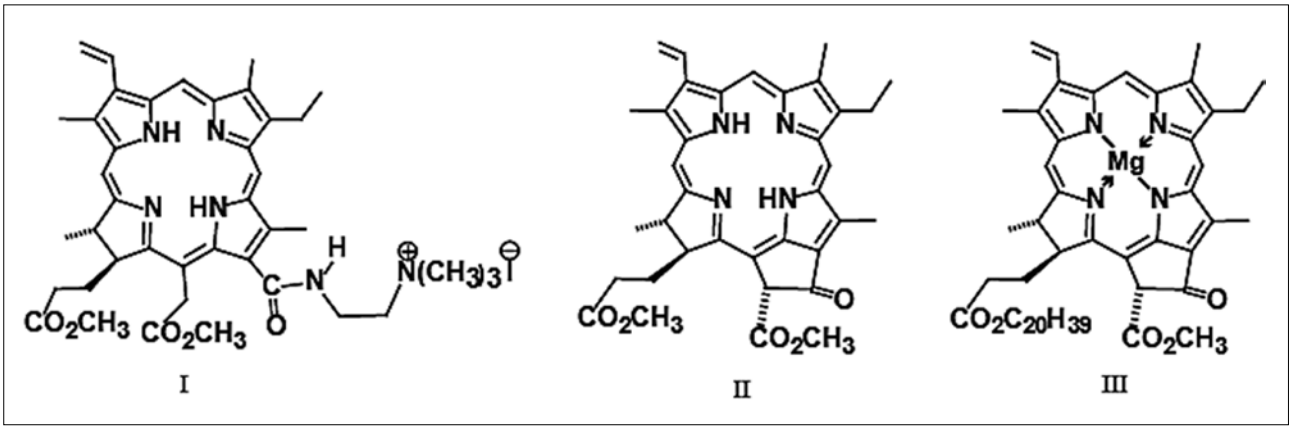

Рис. 1. Объект исследования и природные источники хлорина е6: I – хлорин е6 13(1)-N-(2-N'N'N'-триметиламмониоэтил иодид) амид 15(2), 17(3)-диметиловый эфир (соединение I); II – метилфеофорбид а; III – хлорофилл а.
Fig. 1. Objects of study and natural sources of chlorin e6: I – chlorin e6 13(1)-N-(2-N'N'N'-trimethylammonioethyl iodide) amide-15(2),17(3)-dimethyl ester (comp. I); II – methylpheophorbide a; III – chlorophyll a.

In a preliminary study of the drug in order to select doses for further determination of acute toxicity, 11 outbred female rats weighing from 200 to 230 g participated. The experiment was carried out in November - December.

Two rats were injected with a potential carrier (Tween-80) in 1 ml of 1% and 3% aqueous solution containing 10 and 30 mg of the substance, respectively.

PS solutions were prepared by weight as follows: a weighed portion of solid PS was mixed with the calculated amount of Tween-80, then double-distilled water was slowly added to the resulting viscous mass, the solution was homogenized by ultrasound (Sonopulse ultrasonic homogenizer (Bandelin, Germany)), after which the resulting solutions were centrifuged (3000 rpm) to remove air bubbles.

The thus prepared aqueous solution of the study drug containing various doses of PS in accordance with the table, as well as 1% of the solubilizer Tween-80, was injected into 9 rats (Nos. 1 - 9). The injection volume in all cases was 1 ml. In rats No. 7 and No. 9, the drug was injected intraperitoneally, the rest - in the tail vein (Table).

Animals that received injections of Tween-80, including in amounts exceeding the working concentration of the solubilizer (1%), did not show any behavioral changes during the entire observation period, which indicated a low toxicity of this biocompatible SAS.

In rats that received a cationic chlorin preparation intravenously at a dose of more than 75 mg/kg of body weight, ear hyperemia developed the next day, and no other features associated with the route of administration were noted. One animal (No. 9, which received a dose of 150 mg/kg) died on the second day, an autopsy was performed on the day of death. Euthanasia of the rest of the animals was performed 2 weeks after PS injection by a sharp displacement of the cervical vertebrae, followed by autopsy and sampling of the brain, lungs, heart, liver, and kidneys for histological examination.

Таблица

Величина доз ФС, введенного крысам на первом этапе исследования

Table

The amount of PS doses administered in rats at the first stage of the study

№ животного Number of animal	Доза (мг/кг массы тела) Dose (mg/kg of body weight)
1	5
2	10
3	20
4	30
5	50
6	75
7	100
8	125
9	150

The main experiment, which was conducted in May-June 2021, involved 15 outbred female rats (nursery: Andreevka branch of the Federal State Budgetary Institution of Science "Center for Biomedical Technologies" of the Federal Medical and Biological Agency) weighing from 190 to 220 g.

The animals were divided into 3 groups of 5 rats each. A solution of monocationic chlorin e6 was administered once intraperitoneally in the morning at the following doses: group I - 100 mg/kg, group II - 125 mg/kg, group III - 150 mg/kg of body weight with subsequent observation.

In all dead animals on the day of death, in survivors - 14 days after the injection of monocationic chlorin e6, an autopsy and sampling for subsequent histological examination of the brain, lungs, heart, liver, kidneys and spleen was performed. The slaughter was performed by a sharp displacement of the cervical vertebrae.

After the removal of organs, a histological examination of the autopsy material was performed. In groups II and III, all animals died after 1.5–3 days, in group I, 2 rats died before the end of the experiment, on the 4th and 6th days, respectively. Autopsy of dead animals was carried out within the first day. The three rats that remained alive in group I on the 14th day were subjected to simultaneous decapitation followed by an immediate post-mortem examination. During autopsy, a craniotomy was performed, the entire brain was removed and fixed in 10% neutral formalin solution. One day later, using frontal incisions, the zone of the precentral gyrus of the forebrain, the cerebellum, and the brain stem were isolated. When opening the chest and abdominal cavities, the heart, liver, kidneys, adrenal glands, and spleen were also removed in their entirety and subjected to primary fixation. After secondary fixation and washing of the organ fragments, the material was dehydrated using 99% isopropyl alcohol. Pieces of organs were embedded in paraffin, and histological sections 5–6 μm thick, made on a Microm sledge microtome, were stained with hematoxylin and eosin.

Morphological analysis was carried out on a research microscope "Micros" MS-200, micrographs were obtained using a digital ocular camera DCM 900.

Results and discussion

When conducting a preliminary study on the second day after the injection, a lethal outcome was recorded only in a rat that received the drug at a dose of 150 mg/

kg of body weight, the rest of the animals survived. During the main experiment, almost immediately after the injection, some deterioration in the general condition of the animals was observed: lethargy, drowsiness, muscle weakness. The severity of the described symptoms correlated with the dose of the test compound received and increased with its increase.

Over the next two days, all 10 animals of groups II and III died. In group I, after the administration of the drug, 2 rats died, the death was noted on the 3rd and 6th days. In another rat of group I, during the 5–6th day of the experiment, muscle weakness, shuddering, dishevelled and somewhat dulled hair were noted. In the rest of the animals of group I, no pronounced external changes were observed. Thus, in group I, 2 out of 5 rats died; the PS dose of 100 mg/kg of body weight can be considered close to LD_{50}. For more reliable conclusions, the number of observations should be increased.

During histological examination of the organs, the following data were obtained.

Group I (monocationic chlorin e6 at a dose of 100 mg/kg): in 3 rats that survived until the end of the experiment, moderately pronounced plethora of the postcapillary link of the microcirculatory bloodstream (MCB) was observed in the brain, accompanied by paretic expansion of venules, and perivascular edema of the nervous tissue of cerebral hemispheres. In the cortex of the precentral gyrus and in the cortex of the cerebellum, the stratification of layers is preserved, most of the pyramidal neurons and pear-shaped Purkinje cells with clear contours of the nuclei and cytoplasmic Nissl bodies with a uniform distribution of macroglial elements. The exception is brainstem neurons, some of which have the format of reversible ischemic damage in the form of a decrease in the volume of the cytoplasm, hyperchromia of nuclei, swelling of axons against the background of pericellular edema of the nervous tissue (Fig. 2).

At the macroscopic level, the cavity of the left ventricle of the heart is concentrically narrowed, the right ventricle is moderately dilated, contains liquid blood. Microscopic examination: the lumen of the MCB vessels are dilated, filled with erythrocytes, without signs of aggregation; contractile myocardial fibers of uniform color, with clear contours and cross striation.

Pasty lungs (doughy consistency), occupy 90% of the volume of the pleural cavities. In animals that died on the 3rd and 6th days from the beginning of the experiment, the microscopic picture is characterized by a moderately pronounced plethora of interalveolar septum, spasm of the bronchi of medium and small caliber, the lumens of which are partially or completely obstructed by mucus. In conditions of obstruction of the bronchial apparatus, the formation of foci of centric emphysema is observed (Fig. 3).

Moderately pronounced acute congestion is observed in the kidneys, the anses capillaires of the glomeruli contain erythrocytes, the lumen of the capsule is not expanded, the nephrocytes of the proximal and distal convoluted tubules are of the usual form with a uniform color of the cytoplasm, the lumen of the tubules is free.

Microscopic examination of the liver shows a moderately pronounced plethora of the central and portal veins, the histoarchitecture of the liver acini is preserved, the sinusoids are not dilated, with a free lumen, there are single histiocytes and lymphocytes in the stroma of the portal tracts. In the 2nd and 5th observations, periportal foci of fatty degeneration of hepatocytes with moderate lymphohistiocytic infiltration of the stroma are noted.

Group II (monocationic chlorin e6 at a dose of 125 mg/kg). In the study of the brain in all rats, signs of cir-

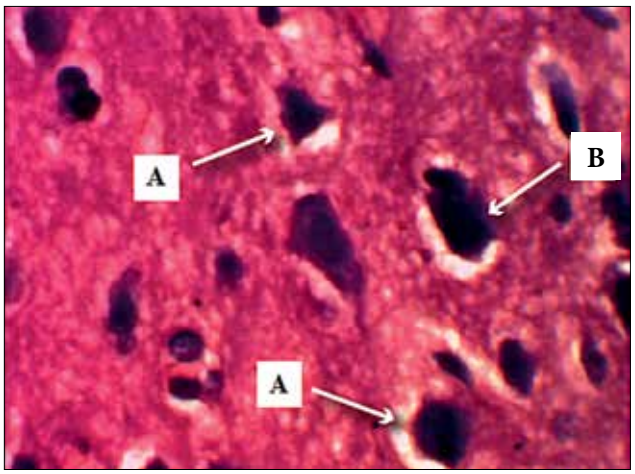

Рис. 2. Гистология. Плазмопикноз, гиперхромия ядер нейронов (А), набухание аксонального отростка нейрона (В). Окраска гематоксилином и эозином. Увеличение 1200.
Fig. 2. Histology. Plasmopyknosis, hyperchromia of neuron nuclei (A), swelling of the axonal process of a neuron (B). Stained with hematoxylin and eosin. Magnification 1200.

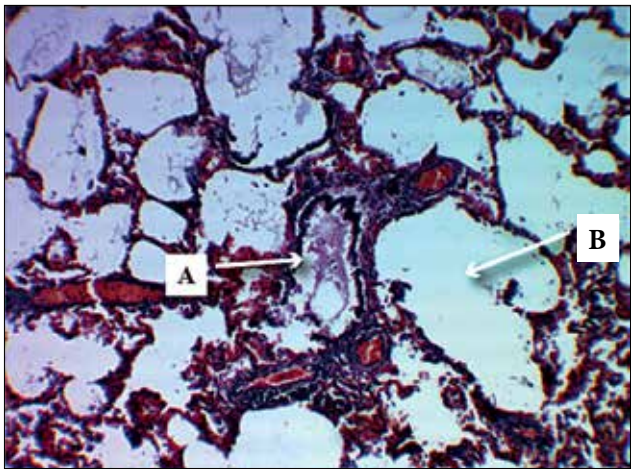

Рис. 3. Гистология. Просвет бронха обтурирован слизью (А), перибронхиальный очаг острой эмфиземы (В). Окраска гематоксилином и эозином. Увеличение 120.
Fig. 3. Histology. Bronchial lumen obturated with mucus (A), peribronchial focus of acute emphysema (B). Stained with hematoxylin and eosin. Magnification 120.

culatory disorders at the MCB level were revealed, which was expressed by aggregation of erythrocytes in the lumen of capillaries, moderately pronounced plethora and dilatation of venules, perivascular and pericellular edema of the nervous tissue (Fig. 4). Focal damage to pyramidal neurons of the cerebral cortex and Purkinje cells (pear-shaped neurons of the cerebellum) was observed, which was expressed by swelling of neurocytes, karyolysis, destruction of cytoplasmic organelles with a perifocal reaction of microglia. Brainstem neurons showed signs of ischemic changes in the form of nuclear hyperchromia with loss of nucleolar contours and a decrease in cell volume.

In the examination of the heart, there was an expansion of the cavities of the right and left ventricles, microscopically in all observations there was a violation of hemocirculation at the level of the microcirculatory bloodstream, which was characterized by aggregation of erythrocytes in the capillaries, plethora of venules, edema of the myocardial stroma. In the subendocardial parts of the myocardium of the left and right ventricles, foci of overcontraction (contractures) were found in the form of wavy contractile fibers with uneven coloring of the cytoplasm of cardiomyocytes.

Acute plethora, edema of the interalveolar septum with deformation and a decrease in the volume of the alveoli were observed in the lungs of experimental animals (Fig. 5).

Under conditions of significant extensive spasm of bronchial tubes and bronchioles, a violation of vascular permeability led to effusion and accumulation of fibrin on the bronchial mucosa in the form of "hyaline membranes".

In the study of the kidneys, moderate plethora of all sections is noted, in 4 observations the nephrocytes of the proximal convoluted tubules were in a state of hydropic (protein) degeneration, tubule lumen were narrowed.

In the liver, acute congestion was expressed by changes mainly in the centers of liver acini, where the central vein and sinusoids of the precentral zone were filled with blood and expanded. Hydropic degeneration of hepatocytes was focal in nature, histoarchitecture of the liver acini was preserved.

Changes in the spleen were characterized by a moderately pronounced plethora of red pulp.

Group III (monocationic chlorin e6 at a dose of 150 mg/kg). In the brain, against the background of hemostasis in the microcirculatory bloodstream vessels, pronounced perivascular and pericellular edema, neuronal damage was characterized by a decrease in cell volume, nuclear hyperchromia, and redistribution of Nissl bodies in the cytoplasm. In the brainstem, changes in single neurons were irreversible with signs of cell necrosis in the form of karyolysis, fragmentation of the cytoplasm, and perifocal reaction of microglia (Fig. 6).

A macroscopic assessment of the heart revealed that the ventricular cavities were dilated, contained liquid blood, the myocardium had a flabby consistency, at the microscopic level, stasis of erythrocytes in capillaries, plethora of intramural veins, and myocardial stromal edema were observed. Focal contractile fibers had wavy changes, individual cardiomyocytes acquired a basophilic color.

The study of the lung tissue showed the presence of a pronounced plethora of the lungs stroma, against which the exudate of plasma proteins led to the formation of eosinophilic films (like hyaline membranes) on the inner surface of the alveoli and bronchial tubes. A pronounced spastic state

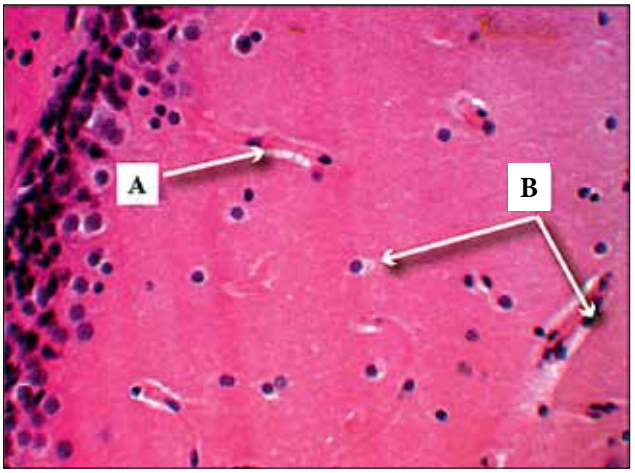

Рис. 4. Гистология. Гемостаз в капиллярах (А), периваскулярный и перицеллюлярный отек нервной ткани (В). Окраска гематоксилином и эозином. Увеличение 480.
Fig. 4. Histology. Hemostasis in the capillaries (A), perivascular and pericellular edema of the nervous tissue (B). Stained with hematoxylin and eosin. Magnification 480.

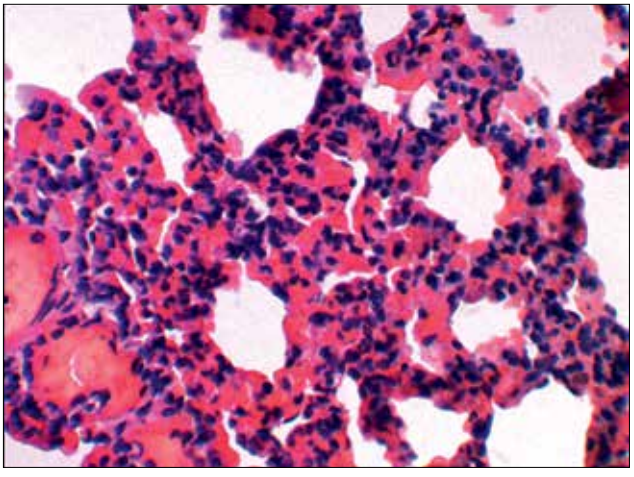

Рис. 5. Гистология. Острое полнокровие легкого, деформация альвеол. Окраска гематоксилином и эозином. Увеличение 480.
Fig. 5. Histology. Acute plethora of the lung, deformation of the alveoli. Stained with hematoxylin and eosin. Magnification 480.

of the bronchi is accompanied by peribronchial cuffing by lymphocytes with single eosinophils (Fig. 7).

In the kidneys against the background of acute venous plethora, hydropic degeneration of the proximal tubules epithelium has become widespread.

Morphological assessment of liver tissue in group III showed pronounced venous plethora of all parts of the liver acinus in the absence of significant damage from hepatocytes.

Changes in the spleen were comparable to the histological picture of plethora in groups I and II.

Thus, changes in the brain, lungs and heart turned out to be morphologically significant. Apparently, the pronounced vasopathic effect of cationic chlorin was the main link in the pathogenesis, as a result of which edema and swelling of the brain progressed. The development of acute vascular encephalopathy was manifested by an increase in general neurological symptoms (at the stage of clinical observations) and correlated with the dose of the administered drug. Irreversible changes in the neurons of the brainstem revealed in rats of groups II and III indicate the development of a dislocation syndrome, which can be considered as the main cause of the death of experimental animals. Pathological evaluation of the lungs revealed widespread bronchospasm with mucus hypersecretion, the severity of which augmented with increasing dose of the drug. A picture of an acute allergic reaction is formed in combination with eosinophilic infiltration of the bronchial walls. The increased permeability of the vascular wall caused the formation of fibrin overlays on the inner surface of the alveoli and small bronchi (like hyaline membranes). Based on the totality of the described changes, it is possible to draw a conclusion about the development of acute respiratory distress syndrome, which has a certain significance in thanatogenesis. Reversible changes in the myocardium are most likely the result of exposure to an arrhythmogenic factor that is formed upon administration of the tested PS. The described morphological changes in the liver, kidneys and spleen in experimental animals are stereotyped in case of intoxication of various nature.

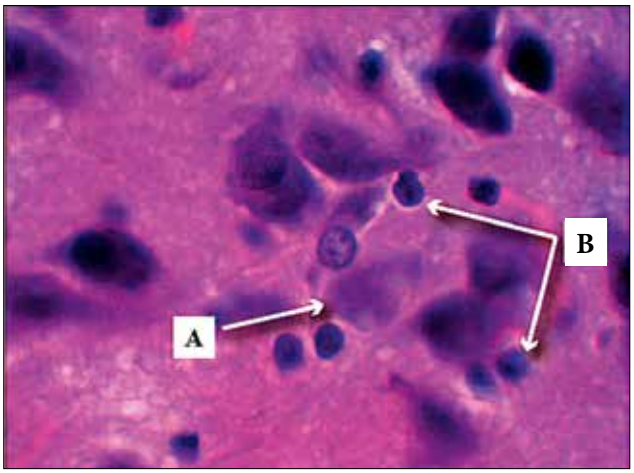

Рис. 6. Гистология. Погибший нейрон продолговатого мозга (A), перифокальная реакция микроглиальных элементов (B). Окраска гематоксилином и эозином. Увеличение 1200.
Fig. 6. Histology. Dead medulla neuron (A), perifocal reaction of microglial elements (B). Stained with hematoxylin and eosin. Magnification 1200.

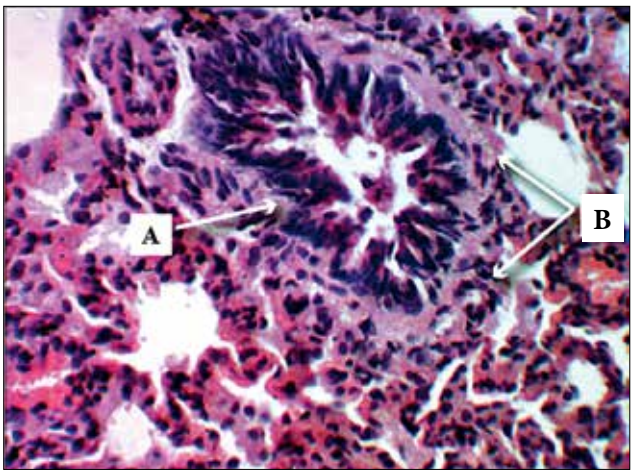

Рис. 7. Гистология. Выраженный бронхоспазм (A), эозинофилы в составе лейкоцитарного инфильтрата (B). Окраска гематоксилином и эозином. Увеличение 480.
Fig. 7. Histology. Severe bronchospasm (A), eosinophils in the leukocyte infiltrate (B). Stained with hematoxylin and eosin. Magnification 480.

Conclusion

1. The value of 100 mg/kg body weight can be considered as a preliminary value of LD_{50} for the studied monocationic chlorin (compound I). It is almost two times higher than that of anionic PS used in clinical practice, however, from a toxicological point of view, it is quite acceptable for continuing preclinical studies, since during PDT the dose of administered PS is usually in the range from 1 to 5 mg/kg. To obtain a more accurate LD_{50} value, the number of laboratory animals should be increased.

2. Intraperitoneal administration of the studied PS in toxic doses causes predominant damage to the brain, lungs, and myocardium.

3. Pathological changes in the vital organs of laboratory animals indicate a pronounced vasopathic effect of compound I with the development of cerebral edema and respiratory distress syndrome, which were the main links of thanatogenesis.

The study was supported by the Russian Science Foundation grant no. No. 21-13-00398, https://rscf.ru/project/21-13-00398/ using the resources of the Research Equipment Sharing Center of the Institute of Chemistry of Solutions of the Russian Academy of Sciences and Ivanovo State University of Chemistry and Technology (with the support of the Ministry of Education and Science of Russia, agreement No. 075-15-2021-671).

REFERENCES

1. Bonnett R. Chemical aspects of photodynamic therapy. *Amsterdam: Gordon Breach Sci. Publ*, 2000, pp. 305.
2. Agostinis P., Berg K., Cengel K.A., Foster T.H., Girotti A.W., Gollnick S.O., Hahn S.M., Hamblin M.R., Juzeniene A., Kessel D., Korbelik M., Moan J., Mroz P., Nowis D., Piette J., Wilson B.C., Golab J. Photodynamic therapy of cancer: an update. *CA Cancer J. Clin*, 2011, Vol. 61(4), pp. 250-281. doi: 10.3322/caac.20114
3. Otvagin V.F., Kuzmina N.S., Krylova L.V., Volovetsky A.B., Nyuchev A.V., Gavryushin A.E., Meshkov I.N., Gorbunova Y.G., Romanenko Y.V., Koifman O.I., Balalaeva I.V., Fedorov A.Y. Water-soluble chlorin/arylaminoquinozoline conjugate for photodynamic and targeted therapy. *Med. Chem*, 2019, Vol. 62(24), pp. 11182-11193. doi: 10.1021/acs.jmedchem.9b01294
4. Van Straten D., Mashayekhi V., De Bruijn H.S., Oliveira S., Robinson D.J. Oncologic photodynamic therapy: basic principles, current clinical status and future directions. *Cancers*, 2017, Vol. 9(19), pp. 1-54. doi: 10.3390/cancers9020019
5. Krammer B., Malik Z., Pottier R., Stepp H. Basic principles. In: Photodynamic therapy with ALA. A clinical handbook / Ed. by Pottier R., Krammer B., Stepp, R. Baumgartner H. *Cambridge: Royal Society Chem. Publ*, 2006, pp. 15-78.
6. Tsyb A.F., Kaplan M.A., Romanko Yu.S., Popuchiev V.V. Clinical aspects of photodynamic therapy. *Kaluga: Publishing house of scientific lit*, 2009, pp. 204.
7. Filonenko E.V., Serova L.G. Photodynamic therapy in clinical practice. *Biomedical Photonics*, 2016. Vol. 5(2), pp. 26-37.
8. Filonenko E.V. Clinical implementation and scientific development of photodynamic therapy in Russia in 2010-2020. *Biomedical Photonics*, 2021, Vol. 10(4), pp. 4-22. doi: 10.24931/2413-9432-2021-9-4-4-22
9. Liu Y., Qin R., Zaat S.A.J., Breukink E., Heger M. Antibacterial photodynamic therapy: overview of a promising approach to fight antibiotic-resistant bacterial infections. *J. Clin. Translat. Res*, 2015, Vol. 1(3), pp. 140-167.
10. Hamblin M. Antimicrobial photodynamic inactivation: a bright new technique to kill resistant microbes. *Curr. Opin. Microbiol*, 2016, Vol. 33, pp. 67-73.
11. Kustov A.V., Berezin D.B., Strelnikov A.I., Lapochkina N.P. Antitumor and antimicrobial photodynamic therapy: mechanisms, targets, clinical and laboratory studies: guidelines / edited by A.K. Gagua. *Moscow: Largo*, 2020, p. 108.
12. Koifman O.I., Ageeva T.A., Beletskaya I.P., Averin A.D., et al. Macroheterocyclic compounds – a key building block in new functional materials and molecular devices. *Macroheterocycles*, 2020, Vol. 13(4), pp. 311-467. doi: 10.6060/mhc200814k
13. Kustov A.V., Privalov O.A., Strelnikov A.I., Koifman O.I., Lubimtsev A.V., Morshnev Ph.K., Moryganova T.M., Kustova T.V., Berezin D.B. Transurethral resection of non-muscle invasive bladder tumors combined with fluorescence diagnosis and photodynamic therapy with chlorin e6-type photosensitizers. *J. Clin. Med*, 2022, Vol. 11, pp. 233. doi: 10.3390/jcm11010233
14. Caterino M., D'Aria F., Kustov A.V., Belykh D.V., Khudyaeva I.S., Starseva O.M., Berezin D.B., Pylina Y. I., Usacheva T. R., Amato J., Giancola C. Selective binding of a bioactive porphyrin-based photosensitizer to the G-quadruplex from the KRAS oncogene promoter. *Intern. J. Biol. Macromolecules*, 2020, Vol. 145, pp. 244-251. doi: 10.1016/j.ijbiomac.2019.12.152
15. Dabrowski J. M. Reactive oxygen species in photodynamic therapy: mechanisms of their generation and potentiation. *Adv. Inorg. Chem*, 2017, Vol. 70, pp. 343-394. doi: 10.1016/bs.adioch.2017.03.002
16. Maisch T. Strategies to optimize photosensitizers for photodynamic inactivation of bacteria. *J. Photochem. Photo-*

ЛИТЕРАТУРА

1. Bonnett R. Chemical aspects of photodynamic therapy // Amsterdam: Gordon Breach Sci. Publ. – 2000. – P. 305.
2. Agostinis P., Berg K., Cengel K.A., Foster T.H., Girotti A.W., Gollnick S.O., Hahn S.M., Hamblin M.R., Juzeniene A., Kessel D., Korbelik M., Moan J., Mroz P., Nowis D., Piette J., Wilson B.C., Golab J. Photodynamic therapy of cancer: an update // CA Cancer J. Clin. – 2011. – Vol. 61(4). – P. 250-281. doi: 10.3322/caac.20114
3. Otvagin V.F., Kuzmina N.S., Krylova L.V., Volovetsky A.B., Nyuchev A.V., Gavryushin A.E., Meshkov I.N., Gorbunova Y.G., Romanenko Y.V., Koifman O.I., Balalaeva I.V., Fedorov A.Y. Water-soluble chlorin/arylaminoquinozoline conjugate for photodynamic and targeted therapy // Med. Chem. – 2019. – Vol. 62(24). – P. 11182-11193. doi: 10.1021/acs.jmedchem.9b01294
4. Van Straten D., Mashayekhi V., De Bruijn H.S., Oliveira S., Robinson D.J. Oncologic photodynamic therapy: basic principles, current clinical status and future directions // Cancers. – 2017. – Vol. 9(19). – P. 1-54. doi: 10.3390/cancers9020019
5. Krammer B., Malik Z., Pottier R., Stepp H. Basic principles. In: Photodynamic therapy with ALA. A clinical handbook / Ed. by Pottier R., Krammer B., Stepp, R. Baumgartner H. // Cambridge: Royal Society Chem. Publ. – 2006. – P. 15-78.
6. Цыб А.Ф., Каплан М.А., Романко Ю.С., Попучиев В.В. Клинические аспекты фотодинамической терапии. – Калуга: Изд. науч. лит. – 2009. – С. 204.
7. Филоненко Е.В., Серова Л.Г. Фотодинамическая терапия в клинической практике // Biomedical Photonics. – 2016. Т. 5, . № 2. – С 26-37.
8. Филоненко Е.В. Клиническое внедрение и научное развитие фотодинамической терапии в России в 2010-2020 гг. // Biomedical Photonics. – 2021. – Т. 10, № 4. – С. 4–22. doi: 10.24931/2413-9432-2021-9-4-4-22
9. Liu Y., Qin R., Zaat S.A.J., Breukink E., Heger M. Antibacterial photodynamic therapy: overview of a promising approach to fight antibiotic-resistant bacterial infections // J. Clin. Translat. Res. – 2015. – Vol. 1(3). – P. 140-167.
10. Hamblin M. Antimicrobial photodynamic inactivation: a bright new technique to kill resistant microbes // Curr. Opin. Microbiol. – 2016. – Vol. 33. – P. 67-73.
11. Кустов А.В., Березин Д.Б., Стрельников А.И., Лапочкина Н.П. Противоопухолевая и антимикробная фотодинамическая терапия: механизмы, мишени, клинико-лабораторные исследования: руководство / под ред. А.К. Гагуа. – М: Ларго. – 2020. – С. 108.
12. Koifman O.I., Ageeva T.A., Beletskaya I.P., Averin A.D., et al. Macroheterocyclic compounds – a key building block in new functional materials and molecular devices // Macroheterocycles. – 2020. – Vol. 13(4). – P. 311-467. doi: 10.6060/mhc200814k
13. Kustov A.V., Privalov O.A., Strelnikov A.I., Koifman O.I., Lubimtsev A.V., Morshnev Ph.K., Moryganova T.M., Kustova T.V., Berezin D.B. Transurethral resection of non-muscle invasive bladder tumors combined with fluorescence diagnosis and photodynamic therapy with chlorin e6-type photosensitizers // J. Clin. Med. – 2022. – Vol. 11. – P. 233. doi: 10.3390/jcm11010233
14. Caterino M., D'Aria F., Kustov A.V., Belykh D.V., Khudyaeva I.S., Starseva O.M., Berezin D.B., Pylina Y. I., Usacheva T. R., Amato J., Giancola C. Selective binding of a bioactive porphyrin-based photosensitizer to the G-quadruplex from the KRAS oncogene promoter // Intern. J. Biol. Macromolecules. – 2020. – Vol. 145. – P. 244-251. doi: 10.1016/j.ijbiomac.2019.12.152
15. Dabrowski J. M. Reactive oxygen species in photodynamic therapy: mechanisms of their generation and potentiation // Adv. Inorg. Chem. – 2017. – Vol. 70. – P. 343-394. doi: 10.1016/bs.adioch.2017.03.002
16. Maisch T. Strategies to optimize photosensitizers for photodynamic inactivation of bacteria // J. Photochem. Photobiol. B: Biol.

biol. B: Biol, 2015, Vol. 150, pp. 2-10. doi: /10.1016/j.jphotobiol.2015.05.010
17. Kobayashi N. Spectroscopically and/or structurally intriguing phthalocyanines and related compounds. Part 1. Monomeric systems. *Izv. Vyssh. Uchebn. Zaved. Khim. Khim. Tekhnol*, 2019, Vol. 62, pp. 4-46. doi: 10.6060/ivkkt.20196206.5913_1
18. Kustov A.V., Smirnova N.L., Berezin M.B. Standard enthalpies and heat capacities of ethyl acetate and deuteroporphyrin dimethylester solution in N,N-dimethylformamide at 298–318 K. *Thermochim. Acta*, 2011, Vol. 521. pp. 224-226. doi: 10.1016/j.tca.2011.02.020
19. Kustov A.V., Smirnova N.L., Berezin D. B., Berezin M.B. Thermodynamics of solution of proto- and mezoporphyrins in N,N-dimethylformamide. *J. Chem. Thermodyn*, 2015, Vol. 89, pp. 123-126. doi: 10.1016/j.jct.2015.05.016
20. Kustov A.V., Smirnova N.L., Berezin D.B., Berezin M.B. Blood porphyrns in binary mixtures of N,N-dimethylformamide with 1-octanol and chloroform: The energetics of solvation, solute-cosolvent interactions and model calculations. *J. Chem. Thermodyn*, 2015, Vol. 83, pp. 104-109. doi: 10.1016/j.jct.2014.12.013
21. Trukhacheva T.V., Shlyakhtin S.V., Isakov G.A. Photolon is a new tool for photodynamic therapy. – Minsk: RUE "Belmedpreparaty". - 2009. – p. 64.
22. Yakavets I., Millard M., Zorin V., Lassalle H.-P., Bezdetnaya L. Current state of the nanoscale delivery systems for temoporfin-based photodynamic therapy: Advanced delivery strategies. *J. Contr. Release*, 2019, Vol. 304, pp. 268-287. doi: 10.1016/j.jconrel.2019.05.035
23. Huang L., Dai T., Hamblin M.L. Antimicrobial photodynamic inactivation and photodynamic therapy for infections. In: Photodynamic therapy. *Methods and protocols / Ed. by Ch.J. New York: Gomer Springer Science+Business Media*, 2010, pp. 155-174.
24. Berezin D.B., Karimov D.R., Venediktov E.A., Kustov A.V., Makarov V.V. The synthesis and singlet oxygen generation study of 13(1)-N-piperazinyl chlorin e6-15(2),17(3)-dimethyl ester. *Macroheterocycles,* 2015, Vol. 8(4), pp. 384-388. doi: 10.6060/mhc151088b
25. Kustov A.V., Belykh D.V., Startseva O.M., Kruchin S.O., Venediktov E.A., Berezin D.B. New photosensitizers developed on a methylpheophorbide a platform for photodynamic therapy: synthesis, singlet oxygen generation and modeling of passive membrane transport. *Pharm. Anal. Acta*, 2016, Vol. 7(5), pp. 480-484. doi: 10.4172/2153-2435.1000480.
26. Venediktov E.A., Tulikova E.Yu., Rozhkova E.P., Belykh D.V., Khudyaeva I.S., Berezin D.B. Synthesis, spectral-luminescent and photochemical properties of a tricationic derivative of chloride e6 with trimethylammonium groups. *Macroheterocycles*, 2017, Vol. 10(3). – pp. 295-300. doi: 10.6060/mhc170404v
27. Kustov A.V., Belykh D.V., Smirnova N.L., Venediktov E.A., Kudayarova T.V., Kruchin S.O., Khudyaeva I.S., D Berezin D.B. Synthesis and investigation of water-soluble chlorophyll pigments for antimicrobial photodynamic therapy. *Dyes Pigm,* 2018, Vol. 149, pp. 553-559. doi: 10.1016/j.dyepig.2017.09.073
28. Kustov A.V., Kustova T.V., Belykh D.V., Khudyaeva I.S., Berezin D.B. Synthesis and investigation of novel chlorin sensitizers containing the myristic acid residue for antimicrobial photodynamic therapy, *Dyes Pigm*, 2020, Vol. 173, pp. 107948. doi: 10.1016/j.dyepig.2019.107948
29. Kustov A.V., Belykh D.V., Smirnova N.L., Khudyaeva I.S., Berezin D.B. Partition of methylpheophorbide a, dioxidine and their conjugate in the 1-octanol/phosphate saline buffer biphasic system. *J. Chem. Thermodyn*, 2017, Vol. 115, pp. 302-306. doi: 10.1016/j.jct.2017.07.031
30. Berezin D.B., Kustov A.V., Krestyaninov M.A., Batov D.V., Kukushkina N.V., Shukhto O.V. The behavior of monocationic

– 2015. – Vol. 150. – P. 2-10. doi: /10.1016/j.jphotobiol.2015.05.010
17. Kobayashi N. Spectroscopically and/or structurally intriguing phthalocyanines and related compounds. Part 1. Monomeric systems // Izv. Vyssh. Uchebn. Zaved. Khim. Khim. Tekhnol. – 2019. – Vol. 62. – P. 4-46. doi: 10.6060/ivkkt.20196206.5913_1
18. Kustov A.V., Smirnova N.L., Berezin M.B. Standard enthalpies and heat capacities of ethyl acetate and deuteroporphyrin dimethylester solution in N,N-dimethylformamide at 298–318 K // Thermochim. Acta. – 2011. – Vol. 521. – P. 224-226. doi: 10.1016/j.tca.2011.02.020
19. Kustov A.V., Smirnova N.L., Berezin D. B., Berezin M.B. Thermodynamics of solution of proto- and mezoporphyrins in N,N-dimethylformamide // J. Chem. Thermodyn. – 2015, Vol. 89. – P. 123-126. doi: 10.1016/j.jct.2015.05.016
20. Kustov A.V., Smirnova N.L., Berezin D.B., Berezin M.B. Blood porphyrns in binary mixtures of N,N-dimethylformamide with 1-octanol and chloroform: The energetics of solvation, solute-cosolvent interactions and model calculations // J. Chem. Thermodyn. – 2015. – Vol. 83. – P. 104-109. doi: 10.1016/j.jct.2014.12.013
21. Трухачева Т.В., Шляхтин С.В., Исаков Г.А. Фотолон – новое средство для фотодинамической терапии. – Минск: РУП «Белмедпрепараты». – 2009. – С. 64.
22. Yakavets I., Millard M., Zorin V., Lassalle H.-P., Bezdetnaya L. Current state of the nanoscale delivery systems for temoporfin-based photodynamic therapy: Advanced delivery strategies // J. Contr. Release. – 2019. – Vol. 304. – P. 268-287. doi: 10.1016/j.jconrel.2019.05.035
23. Huang L., Dai T., Hamblin M.L. Antimicrobial photodynamic inactivation and photodynamic therapy for infections. In: Photodynamic therapy. Methods and protocols / Ed. by Ch.J. New York: Gomer Springer Science+Business Media. – 2010. – P. 155-174.
24. Berezin D.B., Karimov D.R., Venediktov E.A., Kustov A.V., Makarov V.V. The synthesis and singlet oxygen generation study of 13(1)-N-piperazinyl chlorin e_6-15(2),17(3)-dimethyl ester // Macroheterocycles. – 2015. –Vol. 8(4). – P. 384-388. doi: 10.6060/mhc151088b
25. Kustov A.V., Belykh D.V., Startseva O.M., Kruchin S.O., Venediktov E.A., Berezin D.B. New photosensitizers developed on a methylpheophorbide a platform for photodynamic therapy: synthesis, singlet oxygen generation and modeling of passive membrane transport // Pharm. Anal. Acta. – 2016. – Vol. 7(5). – P. 480-484. doi: 10.4172/2153-2435.1000480.
26. Венедиктов Е.А., Туликова Е.Ю., Рожкова Е.П., Белых Д.В., Худяева И.С., Березин Д.Б. Синтез, спектрально-люминесцентные и фотохимические свойства трикатионного производного хлорина e_6 с триметиламмонийными группами // Макрогетероциклы. – 2017. – Т. 10, № 3. – С. 295-300. doi: 10.6060/mhc170404v
27. Kustov A.V., Belykh D.V., Smirnova N.L., Venediktov E.A., Kudayarova T.V., Kruchin S.O., Khudyaeva I.S., D Berezin D.B. Synthesis and investigation of water-soluble chlorophyll pigments for antimicrobial photodynamic therapy // Dyes Pigm. – 2018. – Vol. 149. – P. 553-559. doi: 10.1016/j.dyepig.2017.09.073
28. Kustov A.V., Kustova T.V., Belykh D.V., Khudyaeva I.S., Berezin D.B. Synthesis and investigation of novel chlorin sensitizers containing the myristic acid residue for antimicrobial photodynamic therapy // Dyes Pigm. – 2020. – Vol. 173. – P. 107948. doi: 10.1016/j.dyepig.2019.107948
29. Kustov A.V., Belykh D.V., Smirnova N.L., Khudyaeva I.S., Berezin D.B. Partition of methylpheophorbide a, dioxidine and their conjugate in the 1-octanol/phosphate saline buffer biphasic system // J. Chem. Thermodyn. – 2017. – Vol. 115. – P. 302-306. doi: 10.1016/j.jct.2017.07.031
30. Berezin D.B., Kustov A.V., Krestyaninov M.A., Batov D.V., Kukushkina N.V., Shukhto O.V. The behavior of monocationic chlorin in

chlorin in water and aqueous solutions of non-ionic surfactant Tween 80 and potassium iodide. *J. Mol. Liq*, 2019, Vol. 283, pp. 532-536. doi: 10.1016/j.molliq.2019.03.091

31. Kustov A.V., Krestyaninov M.A., Kruchin S.O., Shukhto O.V., Kustova T.V., Belykh D.V., Khudyaeva I.S., Koifman M.O., Razgovorov P.B., Berezin D.B. Interaction of cationic chlorin photosensitizers with non-ionic surfactant Tween 80. *Mend. Commun*, 2021, Vol. 31(1), pp. 65-67. doi: 10.1016/j.mencom.2021.01.019
32. Shukhto O.V., Khudyaeva I.S., Belykh D.V., Berezin D.B. Aggregation of hydrophobic chlorines with fragments of antimicrobial drugs in aqueous solutions of ethanol and Twin 80. Izvestiya VUZov. *Chemistry and Chemical technology*, 2021, Vol. 64(11), pp. 86-96. doi: 10.6060/ivkkt.20216411.6500
33. Kustov A.V., Garasko E.V., Belykh D.V., Khudyaeva I.S., Startseva O.M., Makarov V.V., Strelnikov A.I., Berezin D.B. Photosensitizers of the chlorin series for antimicrobial photodynamic therapy. *Successes of modern natural science*, 2016, Vol.12(2), pp. 263-268.
34. Berezin D.B., Makarov V.V., Znoyko S.A., Mayzlish V.E., Kustov A.V. Aggregation water soluble octaanionic phthalocyanines behavior and their photoinactivation antimicrobial effect in vitro. *Mend. Commun*, 2020, Vol. 30(5), pp. 621-623. doi: 10.1016/j.mencom.2020.09.023
35. Pylina Ya.I., Khudyaeva I.S., Startseva O.M., Shadrin D.M., Shevchenko O.G., Velegzhaninov I.O., Kukushkina N.V., Berezin D.B., Belykh D.V. Dark and photoinduced cytotoxicity of cationic derivatives of chlorin e6 with different numbers of charged groups. *Macroheterocycles,* 2021, Vol. 14(4). doi: 10.6060/210944b
36. Gushchina O.I., Larkina E.A., Mironov A.F. Synthesis of cationic derivatives of chloride e6. *Macroheterocycles*, 2014, Vol. 7(4), pp. 414-416. doi: 10.6060/mhc140931g
37. Karimov D.R., Makarov V.V., Kruchin S.O., Berezin D.B., Smirnova N.L., Berezin M.B., Zheltova E.I., Strelnikov A.I., Kustov A.V. Optimization of chlorophyll isolation conditions from dioecious nettle (Urtica dioica L.) and spirulina (Spirulina platensis). *Chemistry grows. raw materials*, 2014, Vol. 17(4), pp. 189-196. doi: 10.14258/jcprm.201404310
38. Arzamassev E.V., Guskova T.A., Berezovskaya I.V., Lyubimov B.I., Lieberman S.S., Verstakova O.L. Methodological guidelines for the study of the general toxic effect of pharmacological agents: A guide to the experimental (preclinical) study of new pharmacological agents. *Edited by R.U. Habriev. - M.: Medicine,* 2005, pp. 41-54.

water and aqueous solutions of non-ionic surfactant Tween 80 and potassium iodide // J. Mol. Liq. – 2019. – Vol. 283. – P. 532-536. doi: 10.1016/j.molliq.2019.03.091

31. Kustov A.V., Krestyaninov M.A., Kruchin S.O., Shukhto O.V., Kustova T.V., Belykh D.V., Khudyaeva I.S., Koifman M.O., Razgovorov P.B., Berezin D.B. Interaction of cationic chlorin photosensitizers with non-ionic surfactant Tween 80 // Mend. Commun. – 2021. – Vol. 31(1). – P. 65-67. doi: 10.1016/j.mencom.2021.01.019
32. Шухто О.В., Худяева И.С., Белых Д.В., Березин Д.Б. Агрегация гидрофобных хлоринов с фрагментами антимикробных препаратов в водных растворах этанола и Твин 80 // Известия ВУЗов. Химия и хим. технол. – 2021. – Т. 64, № 11. – С. 86-96. doi: 10.6060/ivkkt.20216411.6500
33. Кустов А.В., Гарасько Е.В., Белых Д.В., Худяева И.С., Старцева О.М., Макаров В.В., Стрельников А.И., Березин Д.Б. Фотосенсибилизаторы хлоринового ряда для антимикробной фотодинамической терапии // Успехи современного естествознания. – 2016. – Т.12, № 2. – С. 263-268.
34. Berezin D.B., Makarov V.V., Znoyko S.A., Mayzlish V.E., Kustov A.V. Aggregation water soluble octaanionic phthalocyanines behavior and their photoinactivation antimicrobial effect in vitro // Mend. Commun. – 2020. – Vol. 30(5). – P. 621-623. doi: 10.1016/j.mencom.2020.09.023
35. Pylina Ya.I., Khudyaeva I.S., Startseva O.M., Shadrin D.M., Shevchenko O.G., Velegzhaninov I.O., Kukushkina N.V., Berezin D.B., Belykh D.V. Dark and photoinduced cytotoxicity of cationic derivatives of chlorin e_6 with different numbers of charged groups // Macroheterocycles. – 2021. – Vol. 14(4). doi: 10.6060/210944b
36. Гущина О.И., Ларкина Е.А., Миронов А.Ф. Синтез катионных производных хлорина e_6 // Макрогетероциклы. – 2014. – Т. 7, № 4. – С. 414-416. doi: 10.6060/mhc140931g
37. Каримов Д.Р., Макаров В.В., Кручин С.О., Березин Д.Б., Смирнова Н.Л., Березин М.Б., Желтова Е.И., Стрельников А.И., Кустов А.В. Оптимизация условий выделения хлорофиллов из крапивы двудомной (Urtica dioica L.) и спирулины (Spirulina platensis) // Химия растит. сырья. – 2014. –Т. 17, № 4. – С. 189-196. doi: 10.14258/jcprm.201404310
38. Арзамасцев Е.В., Гуськова Т.А., Березовская И.В., Любимов Б.И., Либерман С.С., Верстакова О.Л. Методические указания по изучению общетоксического действия фармакологических средств: Руководство по экспериментальному (доклиническому) изучению новых фармакологических средств. / Под ред. Р.У. Хабриева. - М.: Медицина. – 2005. – С. 41-54.

OPPORTUNITIES OF USING ORAL INTRALUMINAL LASER LITHOTRIPSY FOR A LARGE CALCULUS OF THE COMMON BILE DUCT (CLINICAL REPORT)

Ivanov Y.V.[1,2], Sazonov D.V.[1], Smirnov A.V.[1], Mamoshin A.V.[3,4], Baranov A.V.[5], Panchenkov D.N.[2,5]

[1]Federal Scientific and Clinical Center of Specialized Types of Medical Care and Medical Technologies of the FMBA of Russia, Moscow, Russia
[2]Moscow State University of Medicine and Dentistry named after A.I. A.I. Evdokimov" of the Ministry of Health of Russia, Moscow, Russia
[3]Oryol Regional Clinical Hospital, Oryol, Russia
[4]Orel State University named after I.S. Turgenev, Oryol, Russia
[5]Skobelkin State Scientific Center of Laser Medicine FMBA, Moscow, Russia

Abstract

There is a clinical report of successful oral intraluminal laser lithotripsy with subsequent lithoextraction of a large concretion of the common bile duct in a patient with choledocholithiasis and mechanical jaundice. For the intraluminar lithotripsy a tulium laser "Urolaz" was used with energy modes 0,025-0,05-0,1 J, up to a maximum of 0.5 J. The average power is 6-10 W. Laser exposure was carried out by pulses in an aqueous medium in order to prevent carbonation of the light guide and smoke. The effect of exposure to the concretion was manifested in its fragmentation and the formation of small particles without damage of the mucous membrane of the common bile duct. The total duration of the intervention was 45 minutes. The method is effective and safe, thus it avoids the need of endoscopic papillosphincterotomy and violation of the anatomical integrity and physiological function of the Oddi sphincter.

Key words: choledocholithiasis, papillosphincterotomy, fragmentation of concretion, endoscopic laser lithotripsy, common bile duct.

For citations: Ivanov Y.V., Sazonov D.V., Smirnov A.V., Mamoshin A.V., Baranov A.V., Panchenkov D.N. Opportunities of using oral intraluminal laser lithotripsy for a large calculus of the common bile duct (clinical report), *Biomedical Photonics*, 2022, vol. 11, no. 2, pp. 33–38. doi: 10.24931/2413–9432–2022–11-2-33-38.

Contacts: Ivanov Y.V., e-mail: ivanovkb83@yandex.ru

ВОЗМОЖНОСТИ ПРИМЕНЕНИЯ ПЕРОРАЛЬНОЙ ВНУТРИПРОСВЕТНОЙ ЛАЗЕРНОЙ ЛИТОТРИПСИИ ПРИ КРУПНОМ КОНКРЕМЕНТЕ ОБЩЕГО ЖЕЛЧНОГО ПРОТОКА (КЛИНИЧЕСКОЕ НАБЛЮДЕНИЕ)

Ю.В. Иванов[1,2], Д.В. Сазонов[1], А.В. Смирнов[1], А.В. Мамошин[3,4], А.В. Баранов[5], Д.Н. Панченков[2,5]

[1]«Федеральный научно-клинический центр специализированных видов медицинской помощи и медицинских технологий ФМБА России», Москва, Россия
[2]«Московский государственный медико-стоматологический университет им. А.И. Евдокимова» Минздрава России, Москва, Россия
[3]Орловской области «Орловская областная клиническая больница, Москва, Россия
[4]«Орловский государственный университет имени И.С. Тургенева», Орел, Россия
[5]«Государственный научный центр лазерной медицины им. О.К. Скобелкина ФМБА России», Москва, Россия

CASE REPORTS

Резюме

Представлено клиническое наблюдение успешного выполнения пероральной внутрипросветной лазерной литотрипсии с последующей литоэкстракцией крупного конкремента общего желчного протока у пациентки с холедохолитиазом и механической желтухой. Для проведения внутрипротоковой литотрипсии использовали тулиевый лазер «Уролаз» в следующих режимах: энергия – 0,025-0,05-0,1 Дж, максимум до 0,5 Дж. Средняя мощность 6-10 Вт. Лазерное воздействие проводили импульсами в водной среде с целью профилактики карбонизации волокна световода и задымления. Эффект воздействия на конкремент проявлялся в его фрагментации и образовании мелких частиц без повреждения слизистой оболочки общего желчного протока. Общая продолжительность вмешательства составила 45 мин. Метод является эффективным и безопасным, позволяет избежать необходимости выполнения эндоскопической папиллосфинктеротомии и нарушения анатомической целостности и физиологической функции сфинктера Одди.

Ключевые слова: холедохолитиаз, папиллосфинктеротомия, фрагментация конкремента, эндоскопическая лазерная литотрипсия, общий желчный проток.

Для цитирования: Иванов Ю.В., Сазонов Д.В., Смирнов А.В., Мамошин А.В., Баранов А.В., Панченков Д.Н. Возможности применения пероральной внутрипросветной лазерной литотрипсии при крупном конкременте общего желчного протока (клиническое наблюдение) // Biomedical Photonics. – 2022. – Т. 11, № 2. – С. 33–38. doi: 10.24931/2413–9432–2022–11-2-33-38.

Контакты: Иванов Ю.В., e-mail: ivanovkb83@yandex.ru

Introduction

One of the most common complications of cholelithiasis is choledocholithiasis - the presence of stones in the common bile duct. In 10-25% of patients with cholelithiasis, concretion is detected not only in the gallbladder, but also in the common bile duct [1, 2]. The longer the medical history of cholelithiasis, the greater the risk of choledocholithiasis. The presence of stones in the common bile duct against the background of existing cholecystolithiasis or without it, previous cholecystectomy can cause obstructive jaundice or cholangitis, which in itself is an unfavorable factor in the course of the disease. Detected concretion in the common bile duct is subject to mandatory removal, regardless of its presence or absence in the gallbladder due to the risk of developing severe complications: obstructive jaundice, cholangitis, acute gallstone pancreatitis [3].

The clinical picture of choledocholithiasis is quite variable and depends on many factors: the size and number of concretion, the level and degree of blockade of the common bile duct, the topographic anatomy and structure of the terminal section of the common bile duct and the ampulla of the major duodenal papilla (MDP), comorbidities of the organs of the pancreaticoduodenal zone.

In clinical practice, the following manifestations of choledocholithiasis can be found: a) latent, characterized by the absence of a clinical picture of the disease and is detected only during examination of the patient; b) with complete blockade of the common bile duct up to the MDP ampulla, manifested by progressive obstructive jaundice with or without cholangitis; c) with complete blockade of the common bile duct at the level of the MDP ampulla, accompanied by progressive obstructive jaundice and acute pancreatitis; d) with valvular (moving) concretion and stenotic papillitis, periodic unsystematic outbreaks of obstructive jaundice and cholangitis are characteristic; e) choledocho-intestinal fistula with a clinical picture of cholangitis [2].

All existing methods for removing stones from the common bile duct can be conditionally divided into five large groups: 1) upfront surgery (laparotomy, short-scar incision); 2) laparoscopic operations; 3) percutaneous-transhepatic (antegrade) minimally invasive interventions; 4) endoscopic (retrograde) surgical aids; 5) hybrid operations combining several methods of lithoextraction. The use of one or another method of lithoextraction depends primarily on the technical equipment of the hospital, the qualifications of doctors, the characteristics of the clinical picture and the course of the disease.

It has been established that in modern conditions the best way to resolve choledocholithiasis is the endoscopic method, and the "gold standard" of the technique is recognized as endoscopic retrograde cholangiopancreatography (ERCP) and lithoextraction with or without preliminary endoscopic papillotomy/papillosphincterotomy (EPST) [4].

Endoscopic lithoextraction is performed using the Dormia endoscopic grasping basket, which is presented on the medical market with a wide range of reusable and disposable instruments of various shapes, sizes and rigidity. It should be noted that the necessary conditions for the successful removal of a concretion from the common bile duct are a sufficient diameter of the terminal section of the common bile duct and MDP, as well as the possibility of inserting a Dormia basket for a concretion for its full opening and reliable grasping. With small concretion, no more than 1 cm, the procedure for performing ERCP,

EPST and lithoextraction, with sufficient experience of the endoscopist and a typical topographic and anatomical structure of the MDP, usually does not cause technical difficulties and in 92-96% of cases can effectively eliminate choledocholithiasis [4]. The greatest difficulties arise with large and massive stones in the common bile duct. In most cases, unsuccessful attempts to extract large stones from the common bile duct end in a switch to another method of lithoextraction (upfront or laparoscopic surgery). In some cases, the endoscopic method of lithoextraction can lead to a number of specific complications: bleeding after EPST, post-manipulation acute pancreatitis, strangulation of the Dormia basket in the terminal choledochus or MDP, perforation of the common bile duct wall, perforation of the duodenal wall.

In addition to the described technique of intraductal mechanical lithotripsy, balloon dilatation of the area of preliminary EPST followed by lithoextraction or extracorporeal shockwave lithotripsy followed by endoscopic removal of concretion fragments is used in clinical practice with varying degrees of success. The effectiveness of these treatment methods of choledocholithiasis is noticeably inferior to the method of ERCP, EPST and mechanical lithoextraction. Extracorporeal shockwave lithotripsy, due to its low efficiency and high risk of acute cholecystitis, is not considered by most surgeons as an independent method of treating choledocholithiasis.

In recent years, a number of foreign authors recommend using electrohydraulic or laser lithotripsy for large concretion in the common bile duct [5, 6]. The technique of oral transpapillary cholangioscopy and subsequent intraductal laser lithotripsy makes it possible to break stones into small pieces in the common bile duct without damaging its walls, and then remove them using the Dormia basket.

Given the few foreign publications and single reports in the Russian-language medical literature on the implementation of endoscopic laser lithotripsy for choledocholithiasis, we considered it possible to present our own clinical observation.

Clinical observation

Patient A., 56 years old, was hospitalized in the Department of Surgery of the Federal State Budgetary Institution Federal Clinical Research Centre of Russia's Federal Medical-Biological Agency on July 15, 2021 on an emergency basis with a referral diagnosis: obstructive jaundice. From the medical history it is known that in 2017 she underwent laparoscopic cholecystectomy for cholelithiasis, chronic calculous cholecystitis. During the last 6 months before hospitalization, she suffered from periodic pulling pains in the right hypochondrium after eating, which were relieved by antispasmodic drugs. From July 03, 2021, she noticed scleral and skin icteric, from July 08, 2021 - dark urine and discolored feces. Due to the increasing jaundice and the deterioration of the general condition, the patient was referred for hospitalization in a hospital for examination and treatment.

On admission, the general condition of moderate severity. Skin with a pronounced icteric tinge and traces of scratching, there is no clinical picture of cholangitis and acute gallstone pancreatitis. Arterial pressure 130/75 mmHg, pulse 78 beats/min. The abdomen is not swollen, soft, moderately painful in the right hypochondrium and mesogastrium, there are no symptoms of peritoneal irritation. Peristalsis is auscultated, palpation revealed no neoplasms in the abdominal cavity, no ascites. Urination is not disturbed, the urine is dark brown in color, with rectal examination there are traces of light feces.

Blood tests dated July 15, 2021 for hepatitis B and C are negative. Biochemical blood test dated July 15, 2021: total protein 70 g/l, urea 4.7 mmol/l, creatinine 96 μmol/l, total bilirubin 420 μmol/l (direct 378 μmol/l, indirect 49 μmol/l), pancreatic blood amylase 26 U/l, glucose 3.92 mmol/l, AST 390 U/l, ALT 320 U/l, ALP 460 U/l, C-reactive protein 1.6 mg/l. Clinical analysis of urine dated July 15, 2021: dark brown color, relative density 1.39 g/ml, pH 6.5, urobilinoids 2.8 μmol/l, bilirubin 18.5 μmol/l. Indicators of the general blood test, hemostasiograms within normal values.

The patient underwent the necessary instrumental studies. ECG dated July 15, 2021: sinus rhythm, heart rate 76 beats/min, ECA sharply deviated to the left, blockade of the anterior branch of the left branch of the His bundle. X-ray of the chest organs dated July 15, 2021: no pathology. Conclusion from the Ultrasound of the abdominal cavity and retroperitoneal space dated July 15, 2021: choledocholithiasis (a single concretion 20 mm in the terminal section of the common bile duct), signs of biliary hypertension (dilation of the intrahepatic bile ducts up to 5-7 mm, common bile duct up to 21 mm).

On July 16, 2021, under intravenous anesthesia, the patient underwent gastroduodenoscopy (duodenoscope JF-Q150, Olympus), cannulation of the common bile duct. In order to minimize the risk of wirsungography and postoperative pancreatitis, preliminary contrasting of the ductal systems from the mouth of the duodenal duodenum was not performed and was guided by the position of the radiopaque conductor during fluoroscopy. After confirming the location of the conductor in the common bile duct, 5 mm long papillotomy was performed, up to the level of the 1st transverse fold, balloon dilatation of the mouth of the common bile duct with QBD-10x3 balloons (Wilson-Cook) up to 10 mm. With repeated attempts to extract the concretion, it is not possible due to the impossibility of holding the lithoextractor above the concretion and its incomplete coverage by the Dormia basket. It was decided to perform oral cholangioscopy, laser intraductal crushing of the calculus, followed by its lithoextraction.

After replacing the duodenoscope with an ultrathin Olympus GIF-N180 gastroscope with an outer diameter of 4.9 mm, the latter was passed into the duodenum, then into the terminal section of the common bile duct. Due to the high elasticity of this device model, a 0.035"/0.89 mm nitinol conductor wire was used to create rigidity, which was inserted into the instrumental channel of the endoscope.

After the stage of cholangioscopy and visualization of the concretion, the conductor was removed from the lumen of the endoscope, the common bile duct was filled with physiological sodium chloride solution without pressure, followed by its aspiration (Fig. 1). This maneuver in some cases allows "bringing down" the concretion directly to the tip of the endoscope located in the common bile duct.

For laser lithotripsy, a laser optical fiber 200 μm and 400 μm thick was used, which was initially passed into a Teflon catheter 1.5 m long, 1.5 mm in diameter, intended for use with instrumental channels of endoscopes up to 2.0 mm. The catheter had an additional port for fluid supply. The use of such a design makes it possible to protect the instrumental channel of the endoscope from damage by the optical laser fiber, as well as the fiber itself from creases, and makes the position of the laser fiber in the lumen of the bile ducts more manageable.

After passing the catheter through the instrumental channel of the endoscope, liquid was supplied into the lumen of the common bile duct, the optical fiber was removed 5 mm from the lumen of the Teflon catheter and brought directly to the concretion.

To perform intraductal lithotripsy, a Urolaz thulium laser was used in the following modes: energy setting - 0.025-0.05-0.1 J, up to a maximum of 0.5 J. Average power 6-10 watts. It should be noted that the higher the average power, the greater the effect of crushing and heating of the liquid. The higher the energy in the pulse, the greater the crushing effect, but at the same time, the risk of damage to the wall of the common bile duct increases when the laser pulse directly hits it.

Laser exposure was carried out by pulses in an aqueous medium in order to prevent carbonization of the fiber of the light guide and smoke. The effect on the concretion was manifested in its fragmentation and the formation of small particles (Fig. 2). At the same time, there was no damage to the mucous membrane of the common bile duct, despite the sliding of the optical laser fiber from the concretion.

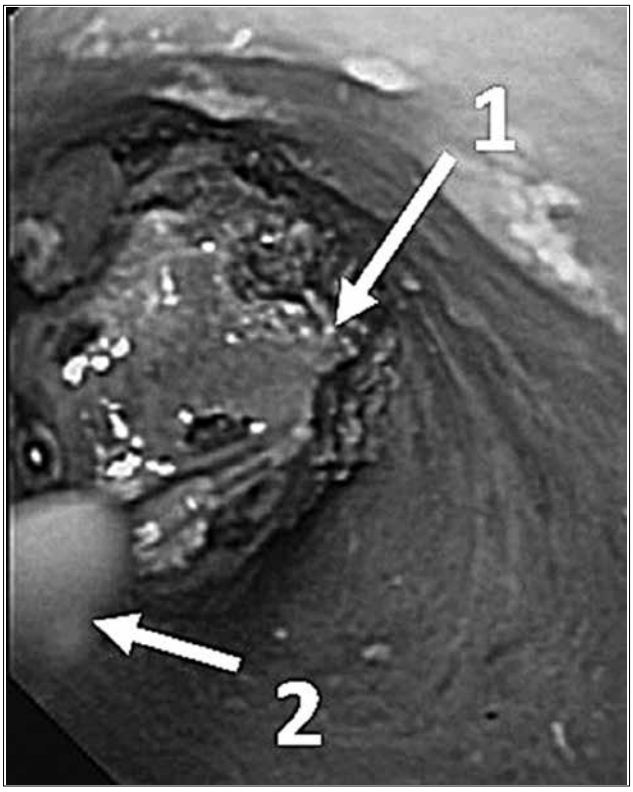

Рис. 1. Этап холангиоскопии и визуализации конкремента в общем желчном протоке: 1 – концевая часть лазерного оптического волокна; 2 – конкремент.
Fig. 1. Cholangioscopy and visualization of the concretion in the common bile duct: 1 – the end part of the laser optic fiber; 2 – concretion.

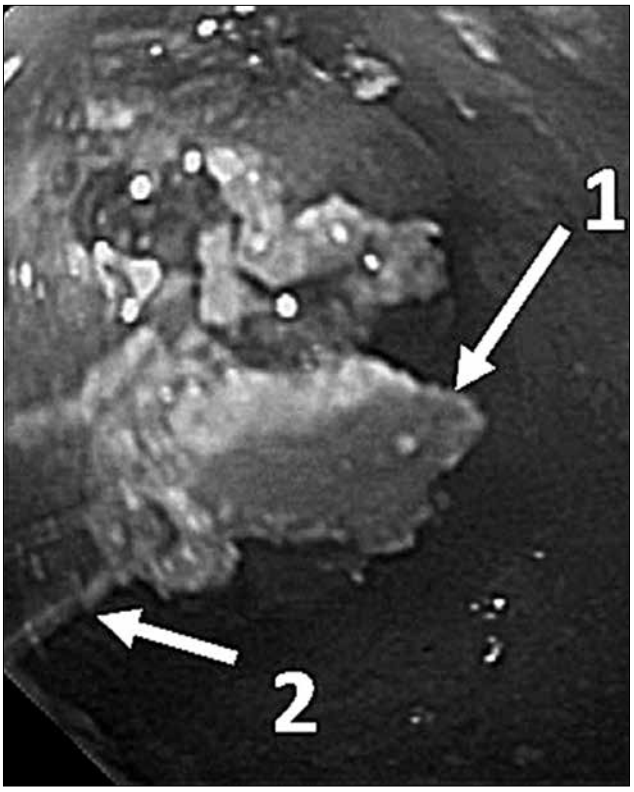

Рис. 2. Этап лазерной литотрипсии:
1 – концевая часть лазерного оптического волокна;
2 – фрагмент конкремента.
Fig. 2. Stage of laser lithotripsy:
1 – end part of the laser optical fiber;
2 – a fragment of a calculus.

The surgical intervention ended with the washing out and extraction of fragments of the concretion with the Dormia basket. The total duration of the intervention was 45 minutes.

The course of the postoperative period is smooth, without complications. The patient was discharged with recommendations from the hospital on July 22, 2021 in a satisfactory condition under the supervision of a surgeon at the place of residence. Total bilirubin on the day of discharge 62 μmol/l (direct 41 μmol/l, indirect 21 μmol/l), AST 80 U/l, ALT 65 U/l, alkaline phosphatase 180 U/l.

Discussion

In recent years abroad, when it is impossible to perform mechanical lithotripsy and lithoextraction from the common bile duct in choledocholithiasis, methods of endoscopic laser or electrohydraulic destruction of large concretion have been used, followed by sanitation of the duct and extraction of fragments with a Dormia basket. The efficiency of laser lithotripsy is slightly higher than electrohydraulic one: 99% and 96.7%, respectively [5, 6].

For the first time, the use of laser technologies began more than 23 years ago in urology for urolithiasis, and then in maxillofacial surgery for sialolithiasis. The mechanism of destruction of concretion by free-running pulses of these lasers is based on the effect of explosive vaporization of concretion, which leads to its uncontrolled fracture into small fragments [7, 8].

For a long time, the main option for intraductal laser lithotripsy was the use of a holmium laser. In 2013–2015 the first publications began to appear on the possibilities of a new type of laser, the operation of which is based on ions of the rare earth metal thulium (No. 69), which, like holmium (No. 67), belongs to the lanthanides [9-12]. However, thulium lasers have a higher degree of absorption of their radiation by water compared to holmium ones. In the domestic medical literature, there are only a few data on the use of laser technologies for choledocholithiasis, so many issues of their technical implementation, indications and contraindications, the choice of optimal operating modes for safe exposure to the bile ducts still require further study [3, 9].

Our first clinical experience with oral intraluminal laser lithotripsy of a large common bile duct concretion using a thulium fiber laser was a complete success. In total, the clinic successfully performed 3 similar surgical interventions for choledocholithiasis (1 clinical case presented above, and 2 observations for acute calculous cholecystitis complicated by choledocholithiasis and cholangitis).

Endoscopic laser lithotripsy of common bile duct concretion followed by lithoextraction allows, if conventional ERCP, EPST and lithoextraction are not possible, to not resort to upfront (laparotomic) surgery or laparoscopic choledochotomy and removal of concretion, which can be technically difficult and not always feasible surgical intervention.

In addition to the undeniable advantages, the method of traditional ERCP, EPST and lithoextraction has its drawbacks. So, to extract large stones from the common bile duct, their preliminary mechanical fragmentation and EPST are necessary. Performing EPST at the height of obstructive jaundice, disorders of the blood coagulation system (high INR, taking anticoagulant drugs, etc.) significantly increases the risk of bleeding and poses a certain threat to the patient's life. There are frequent cases of infringement of the Dormia basket with a captured large concretion in the intrapancreatic part of the common bile duct, which leads to the need to perform an already open surgical intervention to remove the instrument with the concretion. It is not always possible to bring the Dormia basket above the place of obstruction of the common bile duct with a concretion and its capture, and excessive and rough manipulations with the lithoextractor can lead to perforation of the duct wall. Large concretion with a dense structure cannot always be fragmented using the Dormia basket or other lithoextractors.

Another very important fact: EPST, in addition to the risk of bleeding, perforation of the posterior wall of the duodenum leads to the inevitable dysfunction of the sphincter of Oddi, and in some cases to cholangitis.

Oral intraluminal laser lithotripsy makes it possible to fragment a large concretion, even of a dense structure, in a short time frame, while there is no need to perform EPST with all the ensuing risks of its complications. To extract fragments of the concretion from the common bile duct, it is sufficient to perform only papillotomy without destroying the sphincter apparatus of the MDP or balloon dilatation. The risk of complications such as bleeding, perforation of the posterior wall of the duodenum or common bile duct, post-manipulation pancreatitis with endoscopic laser lithotripsy is significantly lower than with traditional ERCP, EPST and lithoextraction. We did not observe these complications when performing oral intraluminal laser lithotripsy.

Conclusion

Thus, endoscopic laser lithotripsy followed by lithoextraction is an effective and safe minimally invasive treatment for choledocholithiasis with large or strangulated concretion in the common bile duct, avoiding the need to perform EPST and disrupting the anatomical integrity and physiological function of the

sphincter of Oddi. A full visual revision of the common bile duct is possible before and after sanitation, the lithotripsy process is carried out under visual control in real time. It is possible to avoid unwanted damage to the wall of the common bile duct and reduce the duration of the intervention due to the targeted bringing of the end of the laser light guide to the surface of the concretion, reduce the risk of complications specific to ERCP and EPST. This technique can be considered as the main method of treating choledocholithiasis, with the ineffectiveness of traditional ERCP, EPST and lithoextraction.

REFERENCES

1. Gutierrez O.I., Bekkali N.L.H., Raijman I., Sturgess R., Sejpal D.V., Aridi H.D. Efficacy and Safety of Digital Single-Operator Cholangioscopy for Difficult Biliary Stones. *Clin. Gastroenterol. Hepatol*, 2018, Vol. 16(6), pp. 918-926. DOI:10.1016/j.cgh.2017.10.017.
2. Komanduri S., Thosani N., Abu Dayyeh B.K., Aslanian H.R., Enestvedt B.K., Manfredi M. Cholangiopancreatoscopy. *Gastrointest. Endosc*, 2016, Vol. 8(2), pp. 209-211. DOI: 10.1016/j.gie.2016.03.013.
3. Hryachkov V.V., Levchenko N.V., Belousov V.V. Targeted contact laser lithotripsy - new opportunities in the treatment of gallstone disease. *Successes of modern natural science*, 2008, No. 5, pp.152-154.
4. Buxbaum J.L., Abbas Fehmi S.M., Sultan S., Fishman D.S., Qumseya B.J., Cortessis V.K. ASGE guideline on the role of endoscopy in the evaluation and management of choledocholithiasis. *Gastrointest. Endosc*, 2019, Vol. 89(6), pp. 1075-1085. DOI: 10.1016/j.gie.2018.10.001.
5. Becker B., Gross A.J., Netsch C. Ho:YaG laser lithotripsy: recent innovations. *Curr. Opin. Urol*, 2019, Vol. 29(2), pp. 103-107. DOI: 10.1097/MOU.0000000000000573.
6. Mutignani M., Dioscoridi L., Italia A., Forti E., Pugliese F., Cintolo M. Thulium laser to manage a difficult biliary lithiasis: a first case report. *Endoscopy*, 2020, Vol.52. (3). pp.112-113. DOI: 10.1055/a-0983- 8278.
7. Enikeev D.V., Glybochko P.V., Okhunov Z., Alyaev Y.G., Rapoport L.M., Tsarichenko D. Retrospective Analysis of Short-Term Outcomes after Monopolar Versus Laser Endoscopic Enucleation of the Prostate: A Single Center Experience. *J. Endourol*, 2018, Vol. 32(5), pp. 17-23. DOI: 10.1089/end.2017.0898.
8. Keller E.X., Coninck V., Vinnichenko V., Chiron P., Doizi S., Guseynov M. Thulium fiber laser for lithotripsy of large renal stones: initial experience. *J. Urology*, 2019, Vol. 201(1), pp. 88. DOI: 10.1097/01. JU.0000555081.fi7fi03.fifi.
9. Budzinsky S.A., Shapovalyants S.G., Fedorov E.D., Vorobyeva E.A., Svirin M.Yu., Malyarov M.G., Chernyakevich P.L., Platonova E.N. The first experience of using a superimpulse fiber tulium laser for contact destruction of stones of the common bile and main pancreatic duct. *Russian Journal of Gastroenterology, Hepatology, Coloproctology,* 2021, Vol.31(2), pp.54-64. DOI: 10.22416/1382-4376-2021-31-2-54-64.
10. McCarty T.R., Sobani Z., Rustagi T. Peroral pancreatoscopy with intraductal lithotripsy for difficult pancreatic duct stones: a systematic review and meta-analysis. *Endosc. Int Open*, 2020, Vol. 8(1), pp. 60-70. DOI: 10.1055/a-1236-3187.
11. Gao B., Bobrowski A., Lee J. A scoping review of the clinical efficacy and safety of the novel thulium fiber laser: The rising star of laser lithotripsy. *Can. Urol. Assoc. J.* 2021, Vol. 15(2), pp. 56-66. DOI: 10.5fi89/cuaj.680fi.
12. Kronenberg P., Traxer O. The laser of the future: reality and expectations about the new thulium fiber lasera systematic review. *Transl. Androl. Urol*, 2019, N8, pp. 398-407. DOI:10.21037/tau.2019.08.01.

ЛИТЕРАТУРА

1. Gutierrez O.I., Bekkali N.L.H., Raijman I., Sturgess R., Sejpal D.V., Aridi H.D. Efficacy and Safety of Digital Single-Operator Cholangioscopy for Difficult Biliary Stones // Clin. Gastroenterol. Hepatol. – 2018. – Vol. 16(6). – P. 918-926. DOI: 10.1016/j.cgh.2017.10.017.
2. Komanduri S., Thosani N., Abu Dayyeh B.K., Aslanian H.R., Enestvedt B.K., Manfredi M. Cholangiopancreatoscopy // Gastrointest. Endosc. – 2016. – Vol. 8(2). – P. 209-211. DOI: 10.1016/j.gie.2016.03.013.
3. Хрячков В.В., Левченко Н.В., Белоусов В.В. Прицельная контактная лазерная литотрипсия - новые возможности в лечении желчно-каменной болезни // Успехи современного естествознания. – 2008. – №5. – С.152-154.
4. Buxbaum J.L., Abbas Fehmi S.M., Sultan S., Fishman D.S., Qumseya B.J., Cortessis V.K. ASGE guideline on the role of endoscopy in the evaluation and management of choledocholithiasis //Gastrointest. Endosc. – 2019. – Vol. 89(6). – P. 1075-1085. DOI: 10.1016/j.gie.2018.10.001.
5. Becker B., Gross A.J., Netsch C. Ho:YaG laser lithotripsy: recent innovations //Curr. Opin. Urol. – 2019. – Vol. 29(2). – P. 103-107. DOI: 10.1097/MOU.0000000000000573.
6. Mutignani M., Dioscoridi L., Italia A., Forti E., Pugliese F., Cintolo M. Thulium laser to manage a difficult biliary lithiasis: a first case report // Endoscopy. – 2020 – Vol.52. (3). – P.112-113. DOI: 10.1055/a-0983-8278.
7. Enikeev D.V., Glybochko P.V., Okhunov Z., Alyaev Y.G., Rapoport L.M., Tsarichenko D. Retrospective Analysis of Short-Term Outcomes after Monopolar Versus Laser Endoscopic Enucleation of the Prostate: A Single Center Experience // J. Endourol. – 2018. – Vol. 32(5). – P. 17-23. DOI: 10.1089/end.2017.0898.
8. Keller E.X., Coninck V., Vinnichenko V., Chiron P., Doizi S., Guseynov M. Thulium fiber laser for lithotripsy of large renal stones: initial experience // J. Urology. – 2019. – Vol. 201(1). – P. 88. DOI: 10.1097/01. JU.0000555081.fi7fi03.fifi.
9. Будзинский С.А., Шаповальянц С.Г., Федоров Е.Д., Воробьева Е.А., Свирин М.Ю., Маляров М.Г., Чернякевич П.Л., Платонова Е.Н. Первый опыт применения суперимпульсного волоконного тулиевого лазера для контактного разрушения камней общего желчного и главного панкреатического протока // Российский журнал гастроэнтерологии, гепатологии, колопроктологии. – 2021. – Т.31, №2. – С.54-64. DOI: 10.22416/1382-4376-2021-31-2-54-64.
10. McCarty T.R., Sobani Z., Rustagi T. Peroral pancreatoscopy with intraductal lithotripsy for difficult pancreatic duct stones: a systematic review and meta-analysis // Endosc. Int Open. – 2020. – Vol. 8(1). – P. 60-70. DOI: 10.1055/a-1236-3187.
11. Gao B., Bobrowski A., Lee J. A scoping review of the clinical efficacy and safety of the novel thulium fiber laser: The rising star of laser lithotripsy // Can. Urol. Assoc. J. – 2021. – Vol. 15(2). – P. 56-66. DOI: 10.5fi89/cuaj.680fi.
12. Kronenberg P., Traxer O. The laser of the future: reality and expectations about the new thulium fiber lasera systematic review // Transl. Androl. Urol. – 2019. – N8. – P. 398-407. DOI:10.21037/tau.2019.08.01.

ПРАВИЛА ДЛЯ АВТОРОВ

Общие требования к представленным материалам

Ответственность Автора

Представленные в работе данные должны быть оригинальными. Не допускается направление в редакцию работ, которые были напечатаны в других изданиях или посланы для публикации в другие редакции. Ответственность за предоставление материалов, полностью или частично опубликованных в другом печатном издании, несет Автор.

Автор гарантирует наличие у него исключительных прав на использование переданного Редакции материала. В случае нарушения данной гарантии и предъявления в связи с этим претензий к Редакции, Автор самостоятельно и за свой счет обязуется урегулировать все претензии. Редакция не несет ответственности перед третьими лицами за нарушение данных Автором гарантий. За достоверность и полноту сведений, изложенных в публикациях, а также за точность информации по цитируемой литературе, несет ответственность Автор статей.

Процедура предоставления статьи в Редакцию

Статьи в редакцию журнала подают через форму на сайте журнала www.pdt-journal.com.

Автору, ответственному за контакты с Редакцией, необходимо пройти на сайте журнала процедуру регистрации, после чего появляется техническая возможность направить статью в редакцию через специальную форму.

Общие требования

Автор, ответственный за контакты с Редакцией, загружает статью на сайт журнала отдельным файлом в формате doc. или docx.

Метаданные необходимо дополнительно внести в отдельную электронную форму.

Текст статьи в прикрепленном файле должен быть набран в текстовом редакторе кеглем 12 пунк-тов через 1,5 интервала, желательно шрифтом Times New Roman Cyr, перенос слов не делается, абзацный отступ – 10 мм. Размеры полей: верхнее и нижнее – 20 мм, левое – 30 мм, правое – 20 мм. Рекомендуемый объем статьи, включая таблицы и литературу – в пределах 12–15 страниц формата А4. Все страницы должны быть пронумерованы.

Титульная страница

Титульная страница должна содержать:

- название статьи (выравнивание по центру, заглавные буквы);
- инициалы и фамилию каждого автора (выравнивание по центру);
- названия организаций, в которых работают авторы (если автор работает и выполнял исследования в нескольких организациях, желательно указывать названия всех организаций), города и страны (выравнивание по центру, названия организаций должны быть даны в соответствии с данными портала e-library, в случае нескольких организаций перед названием каждой указывается порядковый номер в формате верхнего индекса и после фамилии каждого автора также верхним индексом обозначается его принадлежность к определенной организации или организациям);
- резюме статьи в неструктурированном виде (без выделения отдельных разделов) объемом 150–200 слов;
- ключевые слова (5–10 слов);
- контактную информацию для общения читателей с ответственным автором для публикации в свободном доступе (e-mail);
- ссылку на статью для цитирования.

Все вышеперечисленные разделы дублируются на английском языке.

Разделы статьи

Оригинальные статьи должны содержать следующие разделы: введение, материал и методы, результаты, обсуждение (последние два раздела могут быть объединены), заключение. Названия разделов должны быть выделены полужирным шрифтом.

Обзоры литературы могут быть не структурированы.

Аббревиатуры

В тексте следует использовать только общепринятые сокращения (аббревиатуры). Не следует применять сокращения в названии статьи. Полный термин, вместо которого вводится сокращение, следует расшифровывать при первом упоминании его в тексте (не требуют расшифровки стандартные единицы измерения и символы).

Таблицы

Таблицы и текст должны дополнять друг друга, а не дублировать.

Таблицы нумеруются в соответствии с порядком их цитирования в тексте. Каждая таблица должна иметь краткое название и иметь ссылки в тексте (например: табл. 1). Единственная таблица в статье не нумеруется. Заголовки граф должны точно соответствовать их содержанию. Использованные в таблице сокращения подлежат расшифровке в конце таблицы.

Названия таблиц и вся информация в таблицах дублируется на английском языке.

Рисунки

Рисунки должны дополнять имеющиеся в статье таблицы и текст, а не дублировать их.

Фотографии должны быть контрастными, рисунки – четкими. Имеющиеся в статье графики должны быть представлены (возможно, отдельным файлом) в виде таблиц с исходными данными.

На микрофотографиях необходимо указать метод окраски, увеличение.

Рисунки нумеруются в соответствии с порядком их цитирования в тексте. Каждый рисунок должен иметь краткое название и иметь ссылки в тексте (например: рис. 1). Единственный рисунок в статье не нумеруется.

Не следует использовать на рисунках, в том числе на графиках, краткие обозначения, даже расшифрованные в тексте (t, S и др.).

Все подписи к рисункам дублируются на английском языке.

Все текстовые надписи на рисунках также дублируются на английском языке через слэш.

Все статьи, поступающие в редакцию, проходят многоступенчатое рецензирование, замечания рецензентов направляются автору без указания имен рецензентов через личный кабинет на сайте журнала. После получения рецензий и ответов автора редколлегия принимает решение о публикации (или отклонении) статьи.

Редакция оставляет за собой право отклонить статью с направлением автору мотивированного отказа в письменной форме. Очередность публикации статей устанавливается в соответствии с редакционным планом издания журнала.

Редакция журнала оставляет за собой право сокращать и редактировать материалы статьи. Небольшие исправления стилистического, номенклатурного или формального характера вносятся в статью без согласования с автором.

Редакция имеет право частично или полностью предоставлять материалы научных статей в российские и зарубежные организации, обеспечивающие индексацию научных публикаций, а также размещать данные материалы на интернет-сайте журнала.

Представление статьи для публикации в журнале подразумевает согласие автора(ов) с опубликованными правилами.

Полные правила с примерами оформления титульной страницы, рисунков, таблиц и списка литературы, приведены на сайте журнала в разделе «Правила для авторов» https://www.pdt-journal.com/jour/about/submissions#authorGuidelines.

ЖИВАЯ
ЭНЕРГИЯ
СВЕТА

Фоторан e6®

НОВЫЙ РОССИЙСКИЙ ПРЕПАРАТ ДЛЯ ФОТОДИНАМИЧЕСКОЙ ТЕРАПИИ

- Действующее вещество природного происхождения
- Отсутствие аллергических реакций
- Отсутствие гепато и нефротоксичности, низкая фототоксичность
- Быстрое накопление в патологической ткани – 1,5-3 часа
- Длительное хранение без потери активности вещества – 3 года
- Низкая стоимость

ПАРТНЁРЫ:

Национальный медицинский исследовательский центр онкологии

Адыгейский республиканский онкологический диспансер

СККОД

ГБУЗ Челябинский областной клинический центр онкологии и ядерной медицины

По вопросам приобретения

+7 (495) 659-64-93
+7 (499) 726-26-98

ФОТОДИТАЗИН®

[fotoditazin]

фотосенсибилизатор хлоринового ряда

«ФОТОДИТАЗИН®» гель — РУ № ФСР 2012/13043 от 03.02.2012 г.
«ФОТОДИТАЗИН®» концентрат для приготовления раствора для инфузий — РУ № ЛС 001246 от 18.05.2012 г.

«ФОТОДИТАЗИН®» применяется для флюоресцентной диагностики и фотодинамической терапии онкологических заболеваний различных нозологических форм, а так же патологий не онкологического характера в следующих областях медицины:

- дерматология
- гинекология
- урология
- торакальная хирургия
- стоматология
- нейрохирургия
- офтальмология
- травматология и ортопедия
- комбустиология
- гнойная хирургия
- ангиология

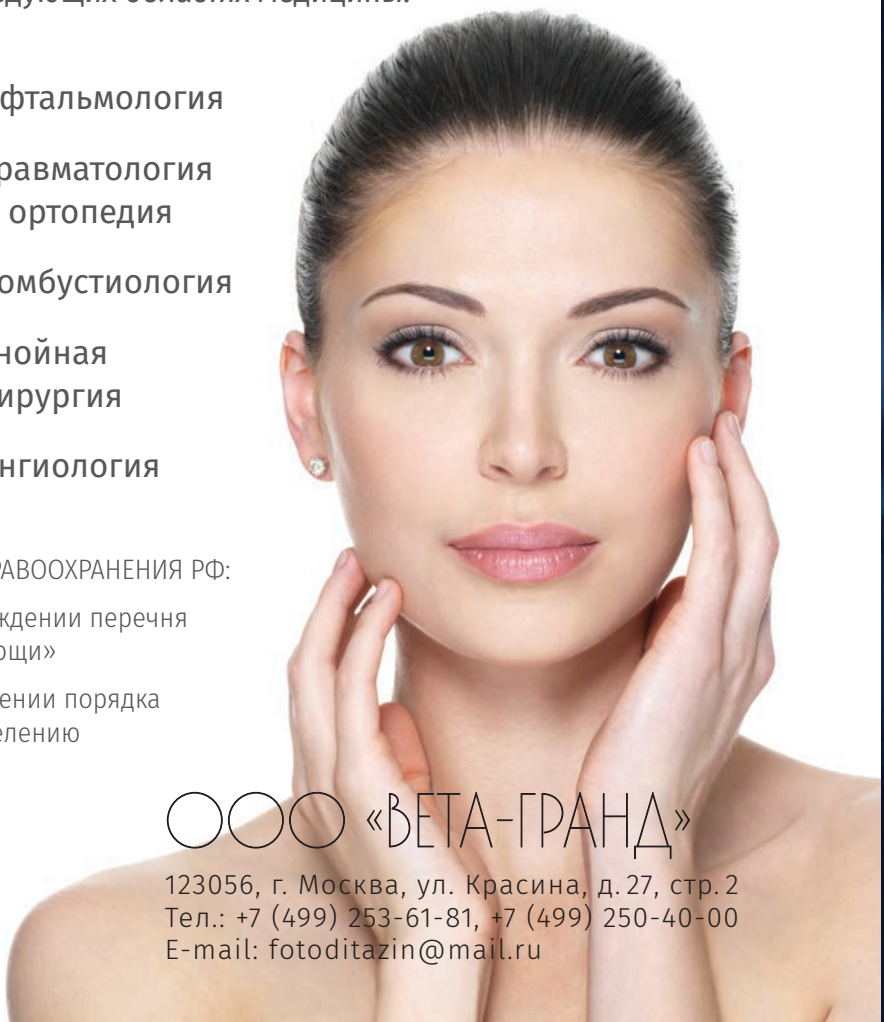

В соответствии с приказами МИНИСТЕРСТВА ЗДРАВООХРАНЕНИЯ РФ:

Приказ № 1629н от 29 декабря 2012 г. «Об утверждении перечня видов высокотехнологичной медицинской помощи»

Приказ № 915н от 15 ноября 2012 г. «Об утверждении порядка оказания медицинской помощи взрослому населению по профилю „онкология“»

www.fotoditazin.com
www.фотодитазин.рф

ООО «ВЕТА-ГРАНД»
123056, г. Москва, ул. Красина, д. 27, стр. 2
Тел.: +7 (499) 253-61-81, +7 (499) 250-40-00
E-mail: fotoditazin@mail.ru